Occurrence and transition probabilities of Omega and High-over-Low blocking

Carola Detring[1,2,], Annette Müller[1], Lisa Schielicke[1], Peter Névir[1], and Henning W. Rust[1]

[1]Institut für Meteorologie, Freie Universität Berlin, Germany
[2]Meteorologisches Observatorium Lindenberg - Richard-Aßmann-Observatorium, Deutscher Wetterdienst, Germany

Correspondence: Carola Detring (carola.detring@dwd.de)

Abstract. Stationary, long-lasting blocked weather patterns can lead to extreme conditions such as anomalously high temperatures or heavy rainfall. The exact locations of such extremes depend on the location of the vortices that form the block. There are two main types of blocking: (i) a *High-over-Low* block with a high located poleward of a single low and (ii) an *Omega* block with two lows that lie south east and south west of the blocking high. In this work, we will introduce a novel method based on the kinematic vorticity number and the point vortex theory that allows to distinguish between these two blocking types. Based on the NCEP-DOE Reanalysis 2 data in the 30-year period from 1990 to 2019 in two regions on the Northern Hemisphere (90°W-90°E and Euro-Atlantic sector 40°W-30°E), we study the trends of the occurrence probability and the onset, offset, and transition probabilities of *High-over-Low* and *Omega* blocking. First, we use logistic regression to investigate the long-term changes of blocking probabilities depending on years, seasons and months. On a yearly basis, our results show only small changes over the 30 years. However, analysing the trends on a monthly basis we find large differences in the occurrence probabilities with significant increases over the 30 year period in February, March and August and a significant decrease in December. The increases can mainly be attributed to an increasing probability of *Omega* blocks. Second, we use a Markov model to calculate the transition probabilities for a two-state model with an *unblocked* and a *blocked* states, and three-state Markov model that additionally distinguishes between the specific blocking types *High-over-Low* and *Omega* blocking. In a Markov model the transition probabilities depend only on the actual and the previous time step neglecting all previous time steps. Over the 30 year period, we find the largest changes in transition probabilities in the summer season, where the transition probabilities towards *Omega* blocks significantly increase, while the unblocked state becomes less probable. Hence, *Omega* blocks become more frequent and stable in summer at the expense of the other states. Moreover, we show that *Omega* blocking is more likely to occur and more persistent than the *High-over-Low* blocking pattern.

1 Introduction

A blocking is a quasi-stationary, persistent large-scale atmospheric flow pattern that blocks the typical westerly flow and forces the jet and embedded pressure systems to bypass on its northern and southern sides (e.g. Rex, 1950). Blocks can last for several days up to weeks. Typically, a minimum blocking duration of 4 to 10 days is assumed (e.g. Rex, 1950; Pelly and Hoskins,

2003; Barriopedro et al., 2006, 2010; Barnes et al., 2011). A block is characterized by a steady high pressure area accompanied by one low pressure area southwards, called *High-over-Low* (dipole), or by two low pressure systems south- and eastwards of the high, called *Omega* block (tripole) (see e.g. Bott, 2012; Woollings et al., 2018). Transitions between the different blocking types can be observed as e.g. documented in Schielicke (2017, appendix A.3, Fig. A69) for summer 2010, where long-lasting blocking caused extreme heat and forest fires over Russia. Due to its persistence, blocks can determine the weather, especially temperature and precipitation pattern. Depending on its location, duration and intensity, these weather situations can have devastating, regional impacts ranging from heatwaves and droughts in the warm season to cold spells in winter and spring (e.g. Pfahl and Wernli, 2012; Brunner et al., 2017, 2018; Russo et al., 2015).

Central European heatwaves, droughts and temperature records in the summer season made the headlines in recent years. In the past years, particularly in 2018 and 2019, a series of blocking led to exceptional, "unprecedented" drought conditions in the two consecutive summers (Hari et al., 2020). *Omega* blocking situations that occurred in June and July 2019 caused widespread temperature records far above 40°C in western and central Europe with an observed record temperature of 45.9°C in southern France at 28 June 2019 (Henley et al., 2019) and 41.2°C in western Germany on 25 July 2019 (Deutscher Wetterdienst, 2020, 2019; Bissolli et al., 2019). In general, a   consists of a long lasting high together with one or two persistent low pressure areas, which can lead to contrary weather situations. For example, the *Omega* blocking that caused the persistent heatwave over Russia in June to August 2010 also led to "record-breaking" floods downstream in Pakistan (e.g. Hong et al., 2011). At the western flank of a quasi-stationary blocking over northern Europe in May/June 2018, an unusual high number of slow-moving thunderstorms caused heavy rain rates and flash floods in large parts of western and central Europe (Mohr et al., 2020).

A conceptual explanation of atmospheric blocking is based on an idealized point vortex model. It was introduced by Obukhov et al. (1984) and further studied in Kuhlbrodt and Névir (2000); Müller and Névir (2014); Müller et al. (2015). It is a Lagrangian formulation of the vorticity equation with vortices conceived as "particles", where, for each vortex, the circulation is conserved.

The motion of a set of point vortices is determined by their circulations and the intervortical distances only, see e.g. Aref (1979); Newton (2001). Hirt et al. (2018) statistically confirm the theory of Müller et al. (2015) that the *Omega* blocking pattern can be regarded as a three point vortex system (tripole) with the anticyclonic point vortex, i.e. the high, located on the poleward side of two cyclonic point vortices. In case these three vortices lie on the vertices of a equilateral triangle and if the sum of all three circulations is zero, the point vortex system *moves* westwards opposing the typical westerly wind of the mid-latitudes. Stationarity of the the vortex system is explained if both speeds are identical. Analogously, a *High-over-Low* block can be described by a point vortex pair (dipole) that moves westward. This concept is summarized in Fig. 1. Applying the point vortex theory allows for the identification and location of each high and the low pressure systems separately. Furthermore, this leads to the possibility to classify and analyse the two blocking states *High-over-Low* and *Omega* blocking types. It should be noted, that this discrete perspective is contrary to the explanation of the blocking based on Rossby-waves as studied by e.g. Tung and Lindzen (1979). Further authors, Tyrlis and Hoskins (2008), Berrisford et al. (2007), Altenhoff et al. (2008) describe the onset of general blockings with the Rossby wave breaking. Using this method based on point vortices provides the opportunity to identify the high and low pressure systems separately. This leads to the first question motivating this present work: Can we find a method to automatically distinguish between the two atmospheric blocking types *High-over-Low* and *Omega* blocks?
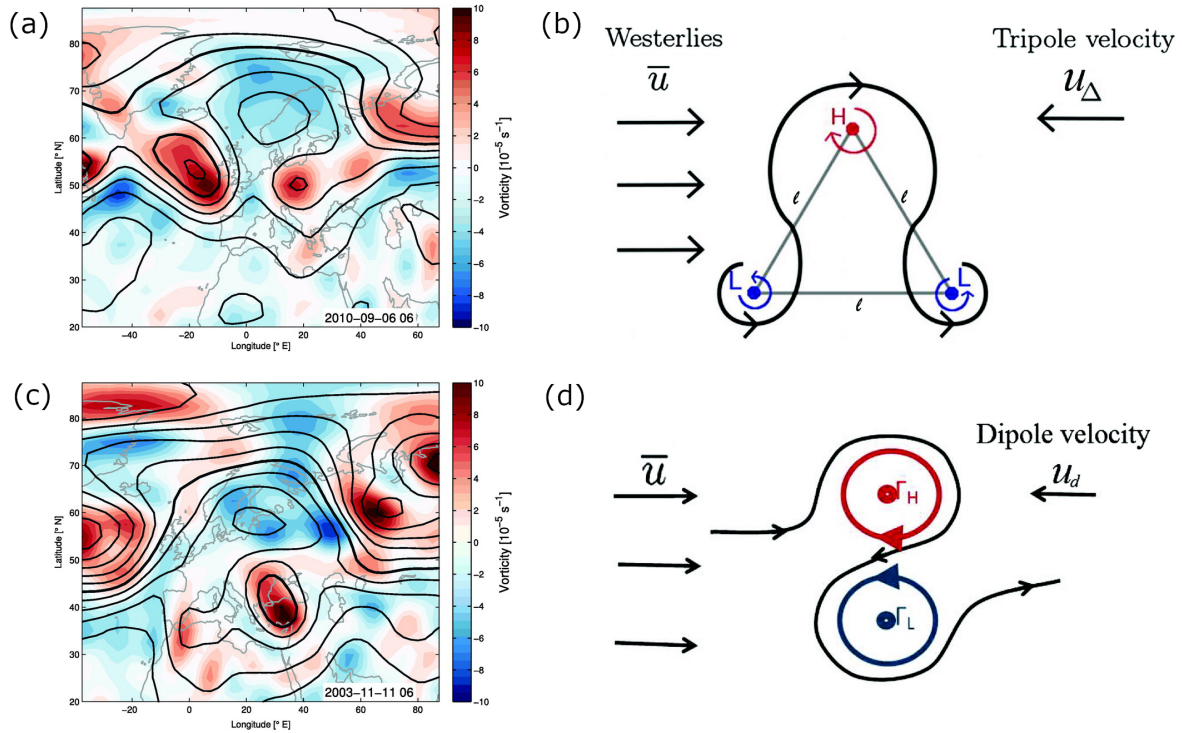
Figure 1. Application of point vortex theory to two distinct atmospheric blocking types:(a),(b): *Omega* blocking (c),(d): *High-over-Low* blocking.(a) and (c): Two exemplary blocking events observed at the 500 hPa level: Displayed is the vorticity (colour-shaded) and contours of geopotential height in 8 dm intervals (bold contour represents 552 dm). (b),(d): Illustration how the corresponding blocking can be realized in the point vortex model. Figure is adapted from Hirt et al. (2018, their figure 2, published under the terms of the Creative Commons Attribution License (http://creativecommons.org/licenses/by/4.0/)) with upper right figure taken from Müller et al. (2015). The point vortex systems become stationary if the westerlies dipole/tripole velocities are of equal magnitude.

The identification of blocking depends on the specific definition and method used. Therefore, blocking climatologies can differ with respect to frequency and location of blocking (e.g. Barriopedro et al., 2010). Although different methods yield different results, they agree in two general aspects: blocking maxima are observed in the North Pacific and North Atlantic-European region, and higher blocking numbers occur in boreal winter compared to the summer season (e.g. Pinheiro et al., 2019). However, larger variability is observed on a block-to-block basis (Pinheiro et al., 2019) and from year-to-year (Davini et al., 2012).

The numerical prediction of blocking onset and persistence, i.e. the transition from zonal to blocked flow and vice versa, is still a challenge. Ferranti et al. (2015) showed that medium-range ensemble forecasts in the Euro-Atlantic region are less skillful in these situations. For a better understanding, transitions between different large-scale weather regimes have been studied by cluster analyses and the application of Markov chains by e.g. Spekat et al. (1983); Egger (1987); Vautard et al.

70 (1990); Kimoto and Ghil (1993). A Markov model describes the probabilities of transitions between the states of a system. For this purpose, only the present state is taken into account. Hence, the future state becomes independent of all previous states except of the current one (e.g. Grewal et al., 2019). Spekat et al. (1983) distinguishes between zonal, mixed and meridional weather regimes in central Europe. They found relatively long residence times within the regimes of 5 to 7 days and relatively low daily transition probabilities of 5 % to 11 % between the regimes. However to the best our knowledge, the transition

75 between different blocking types, i.e. *Omega* and *High-over-Low* blocks, and the unblocked state has not been studied so far on a sub-daily, 6-hourly time scale. On this data basis, we will analyse the occurrence of the different blocking types, tackling the second question if blocking occurrence probabilities undergo long-term changes and if these changes depend on season or month? The third question arises: Do onset (formation), offset (decay) or transition probabilities from one blocking type to another undergo long-term changes? Do these changes depend on season or month? Davini and D'Andrea (2020) compare the

80 blocking frequency for different regions using different models. Analysing the linear trend for the time period 1951-2017, also for seasons, the authors find a large spread among the different models and large dependencies on the region. Analysing the trend of the seasons, the authors find that for the Northern Hemisphere the blocking trend is negative in winter, and positive in summer. Even though their results show a general decrease of blocking frequency in the future, the impact in some regions and seasons, e.g. the summer Ural blocking, might increase. By investigating linear blocking trend for the time period 1980–2012

85 Barnes et al. (2014) show that the blocking trends also depend on the blocking indices and the models. The authors find no general evident increase in blocking over the Northern Hemisphere. But they further show that the results depend on the regions, seasons and also on the analyzed time period. There are significant seasonal increases for some regions, such as Asia (DJF) and the North Atlantic (JJA). Furthermore, Cheung et al. (2013) confirm a strong dependence of the blocking frequency on the seasons. Their results indicate that the strength of blocking events, in terms of intensity and extension, is stronger in

90 winter and weaker in summer. But they also state that the impact of summer blocks might be higher.

To answer the three questions,

1. Can we find a method to automatically distinguish between the two atmospheric blocking types *High-over-Low* and *Omega* blocks?

2. Do blocking occurrence probabilities undergo long-term changes? Do these changes depend on season or month?

95 3. Do onset (formation), offset (decay) or transition probabilities from one blocking type to another undergo long-term changes? Do these changes depend on season or month?

the work is structured as follows. First, we shortly describe the data set and variables that will be used for our analysis in Section 2. In Section 3, we will explain the steps of our method in more detail: This includes the identification of blocking events (Section 3.1) and their properties (Section 3.2). Moreover, the decision process for the blocking types – *High-over-Low*

100 or *Omega* block – is explained in Section 3.3. We use a subset of the blocking data (Section 3.4) in order to analyse the Euro-Atlantic region with respect to the evolution and transition probabilities of blocking. The statistical methods used in the analysis of occurrence probabilities (logistic regression) and for the transition probabilities (Markov processes) are explained

in Sections 3.5 and 3.6. The results will be presented in Section 4 and discussed in Section 5. A final concise conclusion is given in Section 6.

2 Data

We used the NCEP-DOE Reanalysis 2 data set (Kanamitsu et al., 2002) for our analysis. The data has a grid spacing of $2.5° \times 2.5°$ on a regular latitude/longitude grid and is available every 6 hours. In our study, we used a period of 30 years from 1990 to 2019. We restricted the analysis to the 500 hPa level, a level where the divergence of the horizontal wind field is close to zero (Schielicke, 2017). This allows us to apply the principles of point vortex theory that requires incompressible flow, i.e. a zero divergence. The variables used for this study were the geopotential height and the horizontal wind components (U, V) at 500 hPa. We will compare the blocking behaviour in two regions. The first region covers half the Northern Hemisphere from $90° W$ to $90° E$, and the second region is a subset of this larger region covering the Euro-Atlantic area from $40° W$ to $30° E$.

3 Methods and design of study

In the following we describe the data preparation and the methodology for the probabilistic analysis of atmospheric blocking. The steps are summarized in Fig. 2.

3.1 Step 1. Identification of instantaneous blocked longitudes (IBLs) and blocking events

In the first step, we use the *Blocking* plugin (Richling et al., 2015) of the freva system (Freie Universität Berlin Evaluation System, see Freva, 2017) to calculate the so-called instantaneous blocking index. This index is a binary 1d blocking index that determines instantaneous blocked longitudes, short IBLs, for every time step of a data series (here, NCEP-DOE Reanalysis 2). The instantaneous blocking index was developed by Tibaldi and Molteni (1990) and identifies blockings in terms of gradients of the geopotential height with regard to a central reference blocking latitude (CRBL). While the CRBL is fixed to $50° N$ in the original work, the freva Blocking plugin uses a modification (after Barriopedro et al., 2010) that allows for a longitudinally-dependent, temporally-varying CRBL in accordance to the climatological stormtrack. A blocking is identified if the geopotential height gradients on the northern (GHGN) and on the southern (GHGS) side of the CRBL satisfy the following criteria as implemented in Richling et al. (2015):

$$GHGS > \quad 0 \, \frac{gpm}{°N} \quad : \text{corresponding to an easterly directed flow}$$
$$GHGN < -10 \, \frac{gpm}{°N} \quad : \text{similar to a westerly flow} > 8 \text{ m/s} \tag{1}$$

In the calculation performed for this study, the spatiotemporally varying CRBL is determined based on the 30-year climatology (1990-2019) of the 500 hPa geopotential height field. In order to capture blocking that are not directly located at the CRBL, a possible shift (Delta) to the north and south is set to 10 degrees latitude in the plugin configuration table. For each time step,
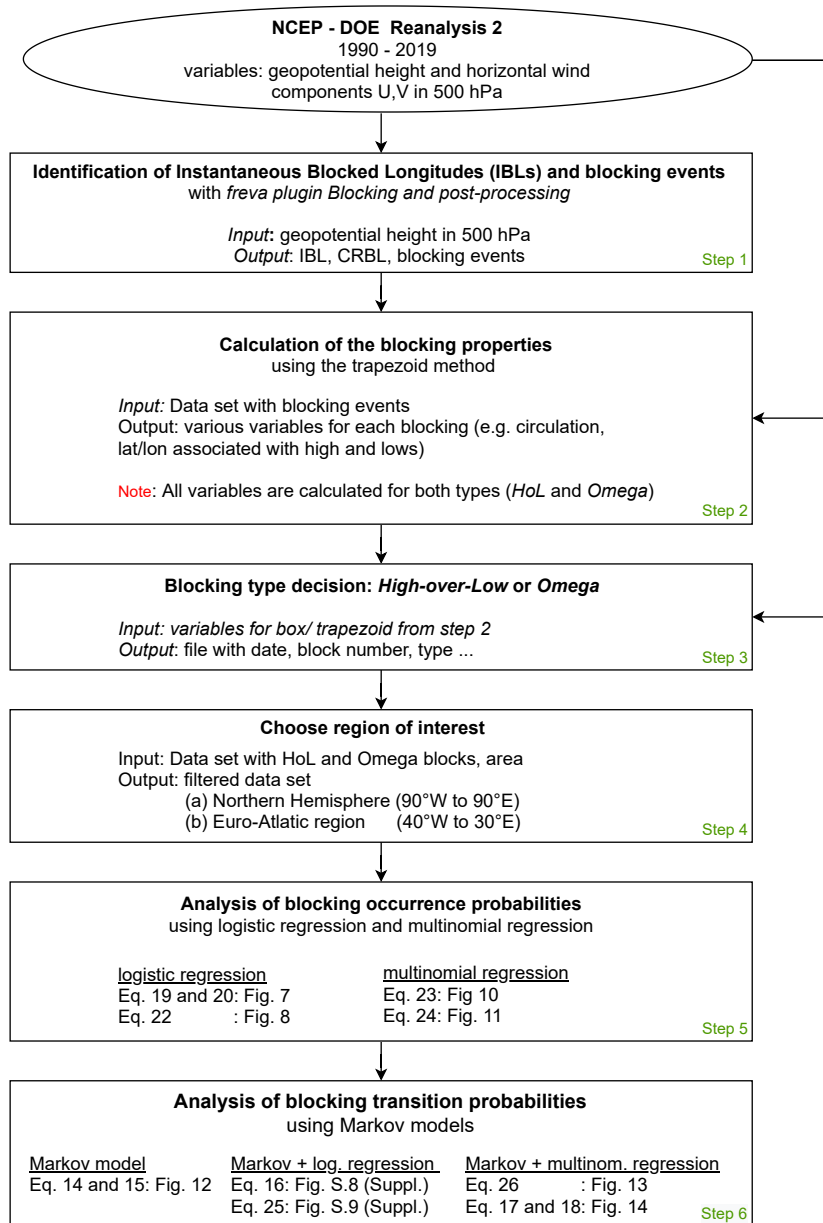
Figure 2. Structure diagram of the individual steps of the evaluation as explained in section 3.

130 we get a (1d) series of longitudes (either 1: blocked or 0: unblocked) that is saved for further analysis. For more details on the method and the specific configurations used in the analysis see the Supplementary Material and Richling et al. (2015).

Prior to the blocking classification, the time series of IBLs is post-processed in the following manner: First, we identify *blocking events* as simply-connected points of IBL = 1 in the time-longitude field. From these blocking events we chose events with a minimum duration of 5 days, i.e. 20 time steps, and a spatial extent of at least 15 degrees longitudes. We only consider

135 Northern Hemisphere blocks in the longitudinal range of $90°\,W$ to $90°\,E$ and north of about $45°\,N$. Note, that we can have two blocking events at the same time in different parts of the area. If this case occurs, the state of the first block is used for the analysis, since only one state can be assigned per time step for the analysis. The second blocking event is discarded.

3.2 Step 2. Calculation of the blocking properties with the trapezoid method

The blocking event list derived in step 1 will be used to search for blocking patterns in the corresponding NCEP Reanalysis

140 fields. For this purpose we applied the trapezoid method (Müller et al., 2015; Hirt et al., 2018) that is able to detect *High-over-Low* and *Omega* blocking patterns using aspects of flow kinematics to identify the vortices as well as point vortex theory to determine blocking properties and to classify the blocking type. The idea behind the trapezoid method is that, in a regular latitude-longitude projection, a *High-over-Low* block resembles a rectangle (or box) surrounding the high and the low while an *Omega* block resembles a trapezoidal shape, where the two lows form the broader base of the trapezoid and the high its

145 smaller top. By assigning specific parts of the trapezoid or box to each low and high, we are able to determine the properties (circulation, location of vortex center) of the associated vortices (cf. Fig. 3 of Müller et al., 2015). The trapezoid method used here is based on the method introduced in Hirt et al. (2018) with slight modifications and the reader is referred to their publication for more details. We will give a brief overview over method here.

The highs and lows are detected by an analysis of the kinematics of the flow. Therefor, we use the dimensionless kinematic

150 vorticity number $W_k = \|\boldsymbol{\Omega}\|/\|\mathbf{S}\|$ (Truesdell, 1953, 1954), which compares the local rates of rotation $\|\boldsymbol{\Omega}\|$ and strain $\|\mathbf{S}\|$ at each grid point. Here, $\boldsymbol{\Omega} = [\nabla\mathbf{v} - (\nabla\mathbf{v})^{\mathbf{T}}]/\mathbf{2}$ and $\mathbf{S} = [\nabla\mathbf{v} + (\nabla\mathbf{v})^{\mathbf{T}}]/\mathbf{2}$ denote the antisymmetric and symmetric components of the velocity gradient tensor $\nabla\mathbf{v}$ that describes the kinematic flow properties around a point. In our case, $\mathbf{v} = (u, v)$ represents the horizontal wind vector. For two-dimensional flow, $W_k = \sqrt{\zeta^2}/\sqrt{2(\partial_x u)^2 + 2(\partial_y v)^2 + (\partial_x v + \partial_y u)^2}$ with ∂_x, ∂_y indicating partial derivatives in x-,y-direction and $\zeta = \partial_x v - \partial_y u$ is the vertical vorticity.

155 For the calculation of $\|\boldsymbol{\Omega}\|$, $\|\mathbf{S}\|$ and W_k, we use the two-dimensional, horizontal wind components of the NCEP reanalysis data set at the 500 hPa level. A vortex is then defined as region of $W_k > 1$, i.e. as an area where the rotation-rate prevails over the strain-rate (see Schielicke et al., 2016; Schielicke, 2017, for further insight and more atmospheric applications). On the other hand, all grid points with values of $W_k \leq 1$ are set to zero to obtain a field of vortex patches. This field can then be multiplied with some field of interest, for example the vertical vorticity field to get areas of positive and negative vorticity, i.e.

160 cyclones and anticyclones. In this field, we search for the anticyclone that lies closest to a duration-weighted IBL[1]. Inside a box

---

[1]This means, that each IBL is assigned with the maximum number of time steps (duration) that this IBL is blocked. For each time step separately, each blocked IBL (either "0" or "1") is multiplied with its maximum duration and the associated longitude. This product is summed up and then divided by the sum of all IBL durations at this time step to get the *duration-weighted* IBL.

bounded by this *duration-weighted* IBL$\pm15°$ longitudes and between $55°$N and $85°$N the grid point with the most negative circulation $\mathbf{P}_{max,neg}$ is identified first. The circulation of a grid point i is given by

$$\Gamma_i = \zeta_i A_i \,, \tag{2}$$

where ζ_i is the vertical vorticity at that grid point and A_i is the area associated with grid point i. It is negative/positive if the vertical vorticity is negative/positive. The circulation of the high Γ_H is calculated as the sum of all grid points N with negative circulation inside a radius of 1500 km around $\mathbf{P}_{max,neg}$ as

$$\Gamma_H = \sum_i^N \Gamma_i \quad \text{for } \Gamma_i < 0 \,. \tag{3}$$

Similar to the point vortex theory the circulation centroid of the high is defined as

$$\mathbf{C}_H = \frac{\sum_i^N \Gamma_i \mathbf{x}_i}{\Gamma_H} \quad \text{for } \Gamma_i < 0 \,, \tag{4}$$

where $\mathbf{x}_i$ is the horizontal coordinate vector of grid point i. Note, that the (positive) circulation and the circulation centroid of a low are calculated in a similar way. The coordinates $(C_{H,x}, C_{H,y})$ of centroid $\mathbf{C}_H$ are finally used to define the rectangle that encloses the high by a fixed distance: $(C_{H,x} \pm 1500\,\text{km}, C_{H,y} \pm 1500\,\text{km})$ which accounts for the typical length scale of a high in the midlatitudes and allows for some deviations from a pure circular shape. The rectangle, that encloses the high, is then extended equatorwards by steps of $2.5°$ latitudes to obtain a box that minimizes the total circulation within the box. The total circulation is defined as the sum of the negative circulation associated with the high and the positive circulation associated with the low. However, only grid points with negative circulation northwards of the low centroid and positive circulation south of the high centroid are taken into account for the calculation of the total circulation. This box shape approximates the *High-over-Low* configuration. At the same time, we search for a minimum of total circulation within a trapezoidal shape, which represents an *Omega* configuration. Therefor, we enlarge the southern boundary of the step-wise changed box symmetrically by steps of $2.5°$ longitudes (on each side) up to a total length of the southern trapezoid boundary of 2.5 times the east-west-length of the box around the high center. The northern boundary remains fixed and only grid points whose centers lie within the trapezoidal shape are counted. Again, only certain areas of the trapezoid are attributed to the high (everything north of the mean latitude of the low centers), to the western low (everything south and west of the high centroid) and the eastern low (everything south and east of the high centroid).

This pattern-like identification is based on the point vortex theory, which states that a system of two or three vortices moves westward if the sum of their circulations is zero, the high lies poleward of the low(s), and the 3-point-vortex-system forms an equilateral triangle (Müller et al., 2015). Note, that we determine the box associated with the *High-over-Low* pattern as well as the trapezoid with the *Omega* pattern for each time step separately. Moreover, for each pattern a number of block properties such as the circulations, and the latitude and longitude associated with the high and the lows (centroids) are derived for later analysis. The decision, which blocking type pattern better fits, is done directly after the calculation of the trapezoid and box shape and is described in the following step 3.

3.3 Step 3. Blocking type decision: *High-over-Low* or *Omega* blocking

For the blocking type decision, the area south of the circulation centroid of the high around the mean latitude of the circulation centroids of the lows (trapezoidal shape derived in step 2) is inspected as follows: A rectangle is centered around the longitude of the high centroid and mean latitude of the lows and split in 3 smaller rectangles where the middle one has a width of 25 degrees longitude and the two outer rectangles are limited by the outline of the trapezoid (see Fig. 3a)[2]. If the mean vertical vorticity inside the middle rectangle (Box 2 in Fig. 3a) is higher than the mean vertical vorticity of all three rectangles together, the time step is defined as *High-over-Low* block; otherwise the time step is defined as *Omega*) block. Finally, we have a time series of each blocking event that can contain both blocking types within a single blocking event (for an example see Fig. 3b and the video in the Supplementary Material). This is a new addition to the trapezoid method in Hirt et al. (2018), who assigned a single blocking type to each whole blocking period. Finally, the time series is once more checked for consistency: In our analysis, a blocking event is expected to consist of the same anticyclone. This is rather a Lagrangian view. Hence, we split the blocking periods to smaller periods, if a certain *distance criterion* is breached: We assume that two highs in successive time steps (6 hours) represent the same system, if their centroid locations differ less than 10 degrees latitude ($\approx 1000\,\mathrm{km}$ in north-south direction) and less than 15 degrees longitude ($\approx 1000\,\mathrm{km}$ in west-east direction). Although we allow for slow motions of the blocks, these "large jumps" rather indicate that a different high pressure system enters the configuration. In order to obtain configurations associated with the same high, we split such periods to two or more smaller periods. If the lifetime of one or both events becomes less than 5 days, the event(s) is(are) removed from the analysis. Of course this reduces the maximum duration of the blocking periods, but is also more consistent with following the block as a system of vortices (instead of a weather regime that characterizes a larger region).

At this point, our method differs from other blocking identification methods that are solely based on indices. In order to better estimate the effect of the distance criterion, we did a number of experiments with different distances (see Table 1). Our initial intent was to bound the distance between high centroids in successive time steps by the typical synoptic-scale Rossby radius $L_D \approx 1000\,\mathrm{km}$. Hence, all experiments are close to this value. For this paper, we will present results for experiment E05 with criterion $\Delta lat = 10°/\Delta lon = 15°$ (if not mentioned otherwise).

3.4 Step 4. Choose region of interest: Euro-Atlantic region and half Northern Hemisphere

The blocking data set derived after applying step 1 to 3 is composed of blocking events that occur between $90°\,W$ and $90°\,E$ with a life time of at least 5 days (= 20 time steps). The detected high centers lie in the mid-latitudes between about $44.5°\,N$ and $83°\,N$. To analyse blocking in Europe in more detail, we separated this data set in a second subset: the Euro-Atlantic sector ranging from $40°\,W$ to $30°\,E$. Since this is a subset of the larger blocking event list, blocks with life times smaller than 5 days can occur in this region. At some point in their life time, these blocks move in or out of the Euro- Atlantic sector.

---

[2]The middle box's width of 25 degrees has been carefully tested in Hirt et al. (2018). At this width, the identified number of *Omega* blocks in comparison to *High-over-Low* blocks were relatively stable. Moreover, the majority of the blocks remained in the same category while changing the box width by some degrees longitude. Hence, we decided to stick to this width in our analysis.
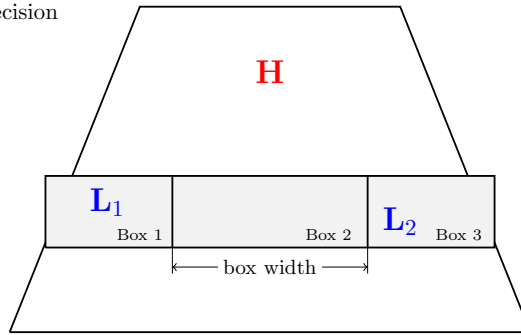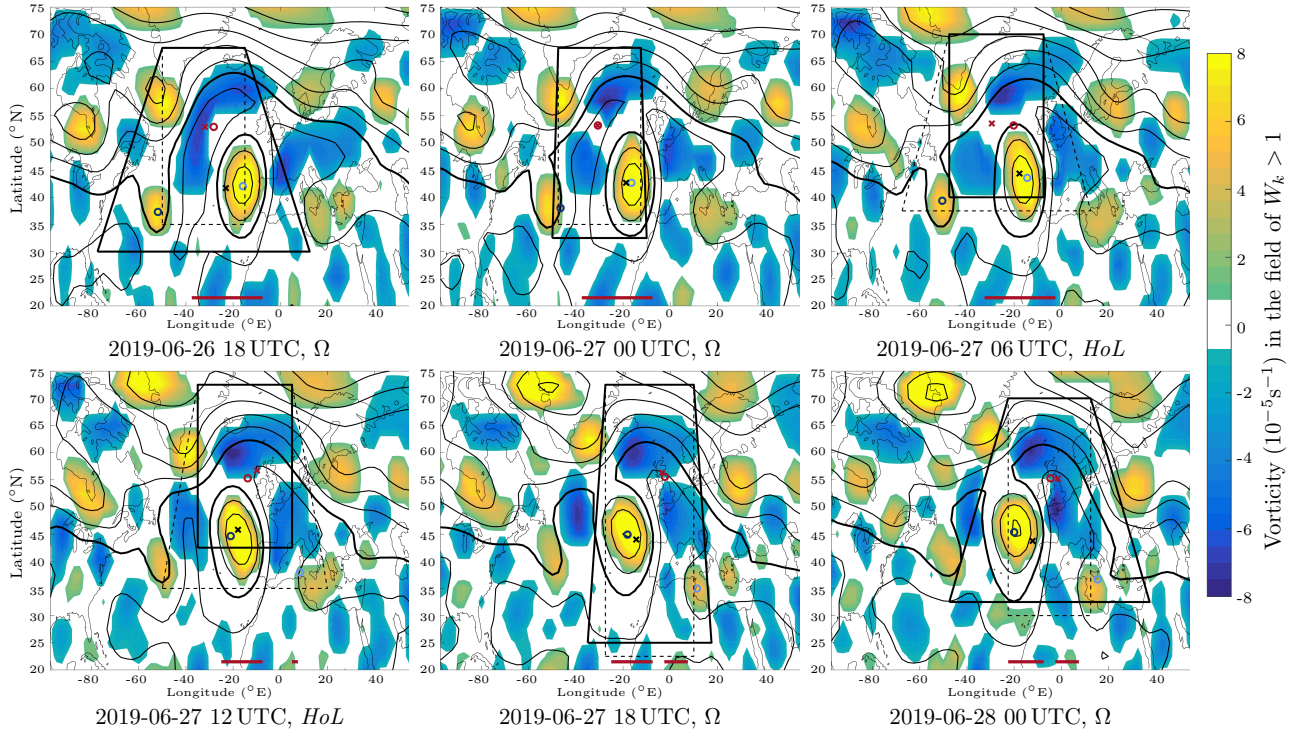
Figure 3. (a) Schematic representation of the blocking type decision based on the trapezoid method. The positive vertical vorticity is calculated for all three boxes, which lie on the mean latitude of the low pressure areas (L_1, L_2). Depending on the magnitude of the mean vorticty in these three boxes, the decision between *High-over-Low* and *Omega* is made. (b) An example blocking event, observed at 26. June 2019 18 UTC - 28. June 0 UTC, is plotted for six time steps that include a transition between *Omega* and *High-over-Low* blocking states. Shaded areas represent the identified vortex field ($W_k > 1$) which is colored by vorticity (in $10^{-5}s^{-1}$; blue: anticyclonic; yellow cyclonic). Black contours are isolines of geopotential height in 80 gpm intervals (thick black   r is the 5840 gpm isoline). The outline of the trapezoid/box is given for each time step, solid shape represent the identified shape; circles (crosses) are the circulation centroids of the identified high (red) and low(s) (blue) for the *Omega* (*High-over-Low*) pattern. The red bar(s) at the bottom of the figures shows the identified IBLs from Step 1. The figures were plotted with help of Matlab (2016) and coastlines were plotted with the built-in Matlab file *coast.mat*. The full time series is given in the Supplementary Material , see also steps 2 and 3.

Table 1. Labeling of experiments with different distance criteria that are used to estimate the uncertainty of the blocking identification method. Longitudes Δlon and Latitudes Δlat are given in degrees.

Δlat: / Δlon:	11°	12°	13°	14°	15°	16°	17°	18°	19°
8°		E04			E25			E26	
10°	E14		E15		E05		E17		E18
12°		E27			E28			E06	

3.5 Step 5. Analysis of blocking occurrence probability using logistic regression

Logistic regression is designed to model probabilities ($0 \le p \le 1$) and is an adequate model to describe blocking occurrence probabilities and their temporal changes for a system that can only yield two states: in our case *blocking* and *no-blocking* patterns. The occurrence probabilities for a system with three possible states: *unblocked* and two distinct blocking states (*Omega* and *High-over-Low*), can be analogously described with multinomial regression. Both are briefly reviewed here.

Logistic regression is a special case of generalized linear models (e.g., Wilks, 2011; Dobson and Barnett, 2008) designed to describe occurrence probabilities depending on a set of external influences (covariates). These covariates can be, for example, time in years as a proxy for climate change, the season or month of occurrence as a proxy for the seasonal cycle, or also large-scale atmospheric flow variables.

The setting can be viewed as a generalization to standard linear models. Let Y_t be a discrete random variable at discrete times t; observations of Y_t are denoted as y_t. The random variable Y_t describes the discrete states of a Markov chain. The two-state model we begin our analyses with, is based on these two states: *no blocking* (nB) and *blocking* (B), observations (coded in integers) can thus only be $y_t = 0$ for nB and $y_t = 1$ for B. The random variable Y_t follows a binomial distribution completely determined by the expectation value which gives the occurrence probability of the blocking event $E[Y_t] = Pr\{Y_t = 1\} = p_t$. The probability of the state *no blocking* is determined by the counter-probability $Pr\{Y_t = 0\} = 1 - p_t$.

Logistic regression describes the dependence of the blocking occurrence probability p_t at time t as a function of covariates $x_{l,t}$ using a log-odds (or logit) link-function

$$\mathrm{logit}(p_t) = \ln\left(\frac{p_t}{1 - p_t}\right) = \beta_0 + \Sigma_{l=1}^{L} \beta_l \, x_{l,t}, \tag{5}$$

with $l = 1, \ldots, L$ covariates $x_{l,t}$ observed simultaneously with y_t and β_l are model parameters to be estimated based on iteratively reweighted least-squares (IRLS). Further details can be found, e.g., in Dobson and Barnett (2008); Wilks (2011). We use the function `glm()` from the package `stats` of the R-environment for statistical computing (R Core Team, 2018).

Rearranging Eq. (5) yields the following expression for the blocking occurrence probability at time t as a function of the covariates $x_{l,t}$:

$$p_t = \frac{1}{1 + e^{-(\beta_0 + \Sigma_{l=1}^{L} \beta_l x_{l,t})}} . \tag{6}$$

In some cases, the influence of one covariate $x_{i,t}$ dependents on the value of another covariate $x_{j,t}$ which can be introduced in a linear model as a so called *interaction* effect $x_{i,t} x_{j,t}$. Think of, for example, the change in blocking occurrence probability with years is dependent on the season, we are looking at. A simple example with *main effects* of two covariates and one *interaction* is

$$\text{logit}(p_t) = \beta_0 + \beta_1 x_{1,t} + \beta_2 x_{2,t} + \beta_3 x_{1,t} x_{2,t}. \tag{7}$$

In the notation for generalized linear models introduced by McCullagh and Nelder (1989) Eq. 7 reads

$$\text{logit}(p_t) \sim x_{1,t} * x_{2,t} \sim x_{1,t} + x_{2,t} + x_{1,t} : x_{2,t}, \tag{8}$$

with $x_{i,t}$ denoting main effects, $x_{1,t} : x_{2,t}$ interaction effects and $x_{1,t} * x_{2,t}$ their commonly used combination. This notation assumes an offset (β_0) being present by default and a parameter β_i to be estimated for each term in the equation. Nota bene: in this notation, the symbols '+', ':' and '*' have special meanings, namely addition of a term in the predictor, interacting effects and combination of both, respectively!

For more than two states, the model can be extended to multinomial logistic regression. We next consider a multinomial random variable Y_t with three states: no blocking (nB), *High-over-Low* (HoL) and *Omega* blocking (Ω). For the multinomial distribution, one probability, e.g. $Pr\{Y_t = nB\} = p_{nB,t}$, is set as reference and the other two $Pr\{Y_t = HoL\} = p_{HoL,t}$ and $Pr\{Y_t = \Omega\} = p_{\Omega,t}$ need to be estimated using

$$\ln\left(\frac{p_{HoL,t}}{p_{nB,t}}\right) \sim x_{1,t} + x_{2,t} + \dots \tag{9}$$

$$\ln\left(\frac{p_{\Omega,t}}{p_{nB,t}}\right) \sim x_{1,t} + x_{2,t} + \dots. \tag{10}$$

The remaining occurrence probability for no blocking can then be derived as $p_{nB,t} = 1 - (p_{\Omega,t} + p_{HoL,t})$. We thus need to solve two regression equations simultaneously. This can be formulated in the framework of (vector) generalized linear models (VGLMs). Parameter estimation is somewhat more cumbersome in this case and realized using iteratively reweighted least squares detailed in (Yee, 2015). Estimation is carried out using the function `vglm()` from the R-package `VGAM` (Yee, 2015). Confidence intervals (95%) are based on asymptotic normality using an interval $[\hat{\theta} \pm 1.96\,\sigma_{\hat{\theta}}]$ around the estimator $\hat{\theta}$ with standard deviation $\sigma_{\hat{\theta}}$.

3.6 Step 6. Analysis of blocking transition probabilities using Markov models

We use Markov models with two and three states to describe transition probabilities between the states related to the different blocking types and the no-blocking state. For both cases, there is thus a discrete set of possible states:

Two-state model: *blocked* (B) and *unblocked* (nB) states,

Three-state model: *High-over-Low* (HoL), *Omega* (Ω) and *unblocked* (nB) states.

The system evolves along a discrete time axis t and can switch between these discrete states. We obtain a *discrete-time Markov chain* on a finite state space. The underlying theory was developed by the Russian mathematician Andrey Andreyevich Markov (For the translated original work see Markov (2006)).

Let Y_t be a sequence of discrete random variables denoting the possible states the Markov chain can be found in, e.g., $Y_t = i$ implies Y being in state i at time t, in general $i \in \{1, 2, 3, \ldots, I\}$, here, $I = 2$ or $I = 3$ for the two-state-model or three-state-model, respectively. We speak of a transition when $Y_{t-1} = i$ changes to $Y_t = j$. Transitions from $Y_{t-1} = i \to Y_t = j$ are described with conditional probabilities which, in general, depend on the history of the process, i.e.

$$p_{ij,t} = P(Y_t = j \mid Y_{t-1} = i, Y_{t-2}, Y_{t-3}, \ldots). \tag{11}$$

Formally, $Y_{t-1} = i \to Y_t = i$ is also called a transition from state i to itself. The Markovian assumption (or Markov property) requires these transition probabilities to depend only on the actual state and not the full history of the process

$$p_{ij,t} = P(Y_t = j \mid Y_{t-1} = i, Y_{t-2}, Y_{t-3}, \ldots) = P(Y_t = j \mid Y_{t-1} = i). \tag{12}$$

This assumption makes handling these processes a lot easier. For *homogeneous* Markov chains, the transition probabilities are independent of external factors or time, i.e. $p_{ij,t} = p_{ij}$, otherwise we speak of a *non-homogeneous* Markov chain. The probability for finding the system at time t in state j, i.e. $Pr\{Y_t = j\}$, is determined by the transition probabilities p_{ij} from all states i into state j weighted with the probability $Pr\{Y_{t-1} = i)$ of finding the system in state i, thus

$$Pr\{Y_t = j\} = \sum_i Pr\{Y_t = j \mid Y_{t-1} = i\} Pr\{Y_{t-1} = i\} = \sum_i p_{ij,t} Pr\{Y_{t-1} = i\}. \tag{13}$$

The simplest Markov Chain is a Bernoulli process consisting of two states, in our case the two-state-model with *no blocking* (nB) and *blocking* (B) ($i, j \in \{nB, B\}$) with transition probabilities given in the transition matrix

$$M_2 = \begin{pmatrix} p_{nB,nB} & p_{nB,B} \\ p_{B,nB} & p_{B,B} \end{pmatrix} \tag{14}$$

with $p_{nB,B} = Pr\{Y_t = B \mid Y_{t-1} = nB\}$. For the three-state-model (*High-over-Low blocking* (HoL), *Omega* blocking (Ω) and *no-blocking* (nB), $i, j \in \{nB, HoL, \Omega\}$), the transition matrix is

$$M_3 = \begin{pmatrix} p_{nB,nB} & p_{nB,HoL} & p_{nB,\Omega} \\ p_{HoL,nB} & p_{Hol,HoL} & p_{HoL,\Omega} \\ p_{\Omega,nB} & p_{\Omega,HoL} & p_{\Omega,\Omega} \end{pmatrix}. \tag{15}$$

Transition probabilities are between 0 and 1 ($0 \leq p_{ij} \leq 1$) and rows sum up to unity, implying that the probability that any of the possible states i is reached at time $t + 1$ is one. Transition probabilities together with the probability distribution of Y_0 (initial distribution) fully describe the Markov chain.

Homogeneous (time-independent) Markov chains can be illustrated using a network diagram. Figure 4 shows an example with two states. The circles describe the different states and the arrows indicate the direction of the transition with the
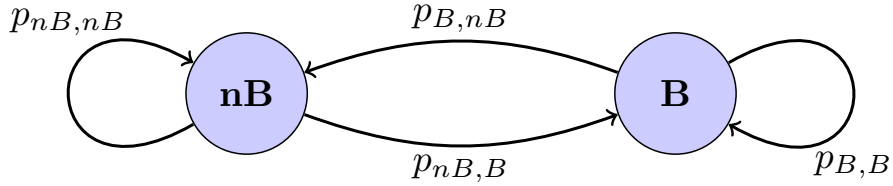
Figure 4. A general example of a network diagram of a homogeneous Markov chain with two states nB (*no blocking*) and B (*blocking*). Arrows indicate transitions and p_{ij} the associated transition probabilities between state i and j with $i, j \in \{nB, B\}$. After Baclawski (2008).

corresponding transition probability p_{ij}. In the homogeneous case, transition probabilities can be estimated from relative frequencies. A more general description of Markov chains and their matrices of transition probabilities can be found in Chap. 9.2 in Wilks (2011). More examples of atmospheric applications of (finite-state) Markov chains can be found in Gottwald et al. (2016, Chapt. 3.4). For further details on homogeneous Markov processes, see e.g.Baclawski (2008).

305   For a non-homogeneous (time-dependent) Markov-process, we use logistic regression to estimate time varying transition probabilities. For the two-state model with *blocking* ($Y_t = B$) and *no blocking* ($Y_t = nB$), we describe transition probabilities changing with Year as

$$\text{logit}(P(Y_t = B \mid Y_{t-1})) \sim Y_{t-1} * \text{Year}, \tag{16}$$

using the notation for generalized linear models as well the parameter estimation strategies introduced above. This results

310   in probabilities for blocking conditioned on being in an unblocked state $Pr\{Y_t = B \mid Y_{t-1} = nB\}$ and conditioned on being in a blocked state $Pr\{Y_t = B \mid Y_{t-1} = B\}$ varying in time. So do their counter probabilities $Pr\{Y_t = nB \mid Y_{t-1} = nB\} = 1 - Pr\{Y_t = B \mid Y_{t-1} = nB\}$ and $Pr\{Y_t = nB \mid Y_{t-1} = B\} = 1 - Pr\{Y_t = B \mid Y_{t-1} = B\}$. Analogously, we can describe time-varying (with Year and season (Seas) or month (Mon)) transition probabilities for the three-state model using multinomial logistic regression, setting the reference to $Pr\{Y_t = nB \mid Y_{t-1}\}$ and

315
$$\ln\left(\frac{Pr\{Y_t = HoL\} \mid Pr\{Y_{t-1}\}}{Pr\{Y_t = nB \mid Y_{t-1}\}}\right) \sim Y_{t-1} * \text{Year} * \text{Seas}, \tag{17}$$

$$\ln\left(\frac{Pr\{Y_t = \Omega\} \mid Pr\{Y_{t-1}\}}{Pr\{Y_t = nB \mid Y_{t-1}\}}\right) \sim Y_{t-1} * \text{Year} * \text{Seas}. \tag{18}$$

Probabilities for all transitions can be derived with the condition $Pr\{Y_t = HoL\} + Pr\{Y_t = \Omega\} + P\{Y_t = nB\} = 1$. For details on main and interaction effects with categorical terms in the predictor, see Wilks (e.g., 2011); Dobson and Barnett (e.g., 2008).

4 Results

In order to answer the research questions asked in the introduction the results are divided into four subsections. First, we will study the uncertainties of the method and give an overview of the total number and duration of blocking for the chosen experiment settings. Then, the temporal development of blocking probabilities for yearly, seasonal and monthly changes of the two-states Markov model (*blocking, no blocking*) are taken into account. In the third subsection the same analysis is done for three-states Markov model (*no blocking, Omega, High-over-Low*). In the last part the transition probabilities of two and three states for the 30 year period are discussed in general. These transitions are also analyzed and shown with respect to their temporal evolution.

4.1 Uncertainty estimates of the identification method and general overview of block properties

In order to better estimate the uncertainty of the identification method, we use a number of experiments with different distance criteria between the high centroids of subsequent time steps (see Table 1). We will take a closer look at some general blocking properties such as their duration and their number and how these are affected by the distance criterion. Generally, the total number of blocks as well as the mean blocked days per year are lower for stricter distance criteria and increase almost linearly with relaxing the criterion (Fig. 5b,c). Thereby, the longitudinal distance is the driving mechanism, while a change in the latitudinal distance criterion only leads to slight differences (e.g. compare experiments E05, E28 and E25 in Fig. 5b,c which differ by $2°$ to $4°$ latitudes, but have the same longitudinal distance criterion).

In the 30-year period from 1990 to 2019 in the region $90°\,W$ to $90°\,E$, we detect a total of 389 blocks ($\approx$13 blocks per year) that lasted for five or more days (see Fig. 5a, blue columns) with an average of about 94 blocked days per year (92 ± 16 for all experiments).For all considered experiments, we observe a mean ($\pm$ standard deviation) of 381 ± 52 blocks in total in this period (or 12.7 ± 1.7 blocks per year), i.e. the variability of block numbers is about 14%. Out of the 389 blocks, the Euro-Atlantic region ($40°\,W$ to $30°\,E$) was affected by 289 blocks (284 ± 40 blocks in total for all experiments) for at least some of the lifetime of the blocks with an average of about 55 blocked days per year (53 ± 9 for all experiments). Since the Euro-Atlantic blocks are a subset of the blocks that occur in the larger region, blocking lifetimes can be smaller than 5 days. However, only 87 of the 289 blocks remained less than 5 days in the Euro-Atlantic region, while the majority affected the region for 5 to 8 days (153 blocks, see Fig. 5a, green columns). Since blocks are observed to be quasi-stationary with usually low travel speeds, the small number of short-lived blocks in the Euro-Atlantic region probably start or end close to the region boundaries and move either in or out of the region during their life time.The mean duration of the blocks is 7.25 days for the larger region, and 5.70 days for the Euro-Atlantic region (red vertical lines in Fig. 5a). Considering all experiments, the mean duration is 7.19 ± 0.30 days for $90°\,W$ to $90°\,E$, and 5.62 ± 0.15 days for $40°\,W$ to $30°\,E$, i.e. the variability in the mean duration is only about 1 time step (6 hours) between all considered experiments. The inner-quartile range (IQR, purple boxes in Fig. 5a) of the different experiments remains relatively consistent up to a duration of 8 days for the Euro-Atlantic region with $IQR = 5.3$ blocks per class. For this region, the largest disagreement between the experiments is found for blocks with a duration between 8 and 9 days with $IQR = 16.5$ blocks. Interestingly in the larger region, the lowest IQR of 4 blocks is
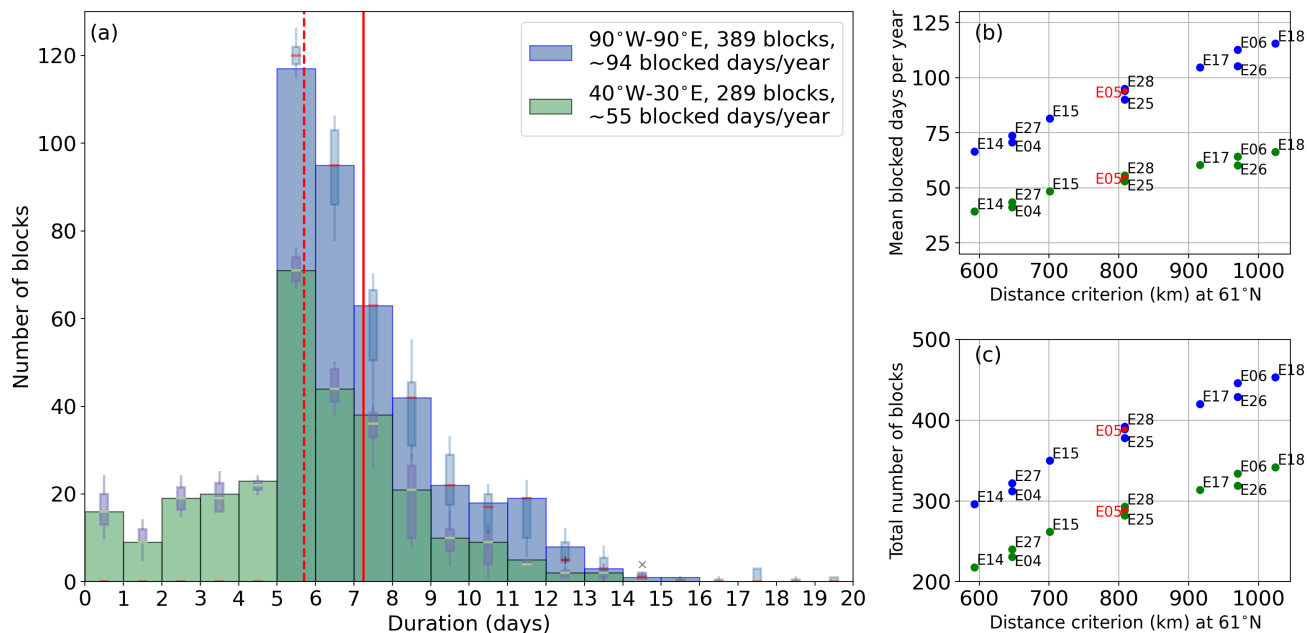
Figure 5. (a) Histogram of the duration of all blocking events in the period 1990-2019 for two selected regions. Blue (green) columns represent the region $90°W$ to $90°E$ ($40°W$ to $30°E$) for experiment E05 with a total of 389 identified blocks (289 blocks); red solid (dashed) vertical lines indicate the mean of this data set. Boxplots on top of the bars show the range of the identified block numbers given by different distance criteria (see Table 1). Boxes indicate the inner-quartile range; whiskers extends to 1.5 times the inner-quartile range; the "x" is an outlier (larger region). (b) Mean blocked days per year and (c) total number of identified blocks in the period 1990-2019 in dependence of the distance criterion. Here the distance criterion was calculated by the longitude criterion of the respective experiments at $61°N$, which is the mean latitude of all identified highs.

found in the class with the highest block number with a duration between 5 and 6 days. In all other classes, the experiments differ more strongly with $IQR \approx 12$ blocks on average for lifetimes between 6 and 12 days. The number of blocks is sensible to the distance criterion (Fig. 5c) which leads to splits of the IBL-detected blocking periods into two or more smaller periods

355 and can hence increase (or decrease, if the new periods are less than 5 days) the overall number of blocks. In terms of averaged blocked days per year (Fig. 5b), the standard deviations is 16 days for the larger region and 9 days for the smaller one. These values account for a fraction of 0.05, and 0.025, respectively, of additionally (or less) blocked days per year.

The temporal development of the blocking frequency and duration for the half Northern Hemisphere and the Euro-Atlantic sector is shown in Fig. 6.

360 In both regions, we observe over the 30 years no clear trend in the frequency of detected blocking events, however, the observed year-to-year variability is high (see black squares in Fig. 6a,b). Additionally the variability between the different experiments is relative large, although this spread shows no trend over time, too (see gray boxes in Fig. 6a,b). Since the block
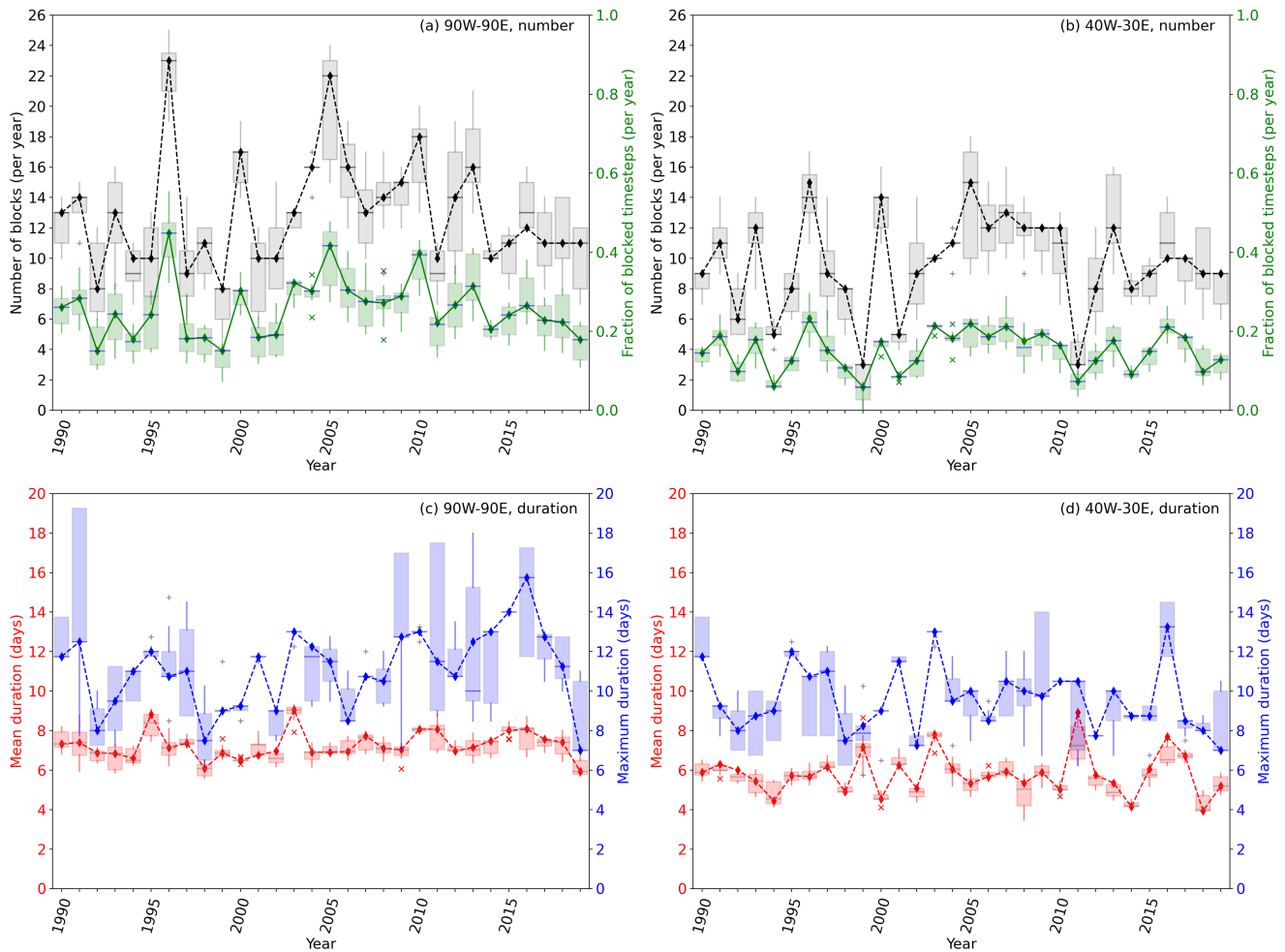
Figure 6. Temporal development of (a,b) blocking number (black) and fraction of annual blocked time steps (green); (c,d) mean (red) and maximum (blue) duration of a blocking event (a,c) for the whole domain ($90° W$ to $90° E$) and (b,d) for Euro-Atlantic region ($40° W$ to $30° E$). Boxes represent the inner-quartile range of the experiment   ibed in Table 1 to test the uncertainty of the method for different distance criteria between two time steps. The whiskers are 1.5 times the inner-quartile range and single points in appropriate colors represent outliers. Note, that blocking numbers are given as integer. Experiment E05 is explicitly plotted in corresponding colors to the boxplots by symbols and lines. These lines are just plotted to ease the identification of E05.

numbers are given by integers, the boxes can be very large. Considering the fraction of blocked time steps per year (green, Fig. 6a,b), the year-to-year variability is still obvious. However, the spread between the experiments is smaller. No trend is observed, neither in the values of experiment E05 (corresponding to the lines in Fig. 6) nor in the spread of all experiments. However, the spread is smaller in the Euro-Atlantic region (Fig. 6b) compared to the larger Northern Hemisphere region (Fig. 6a). With respect to the blocking lifetimes, we observe a very high year-to-year and intra-experimental variability for the maximum duration (blue, Fig. 6c,d) in both regions. This maximum is of course only one data point per year and experiment. Therefore, the spread between the experiments is very large, but smaller for the Euro-Atlantic region. On the other hand, the mean duration remains relatively stable over the 30 year period for E05 as well as for all experiments considered (red, Fig. 6c,d), although the year-to-year variability is larger in the smaller domain. Note, that the residence time of blocks in the smaller region also depends on the travel speed of the blocking and a larger variability in the mean duration could be caused by a year-to-year variability of faster or slower travel speeds.

4.2 Temporal development of blocking probabilities – Two-states blocking model

4.2.1 Seasonal blocking probability

Figure 7 shows the temporal evolution of blocking probability, i.e. the probability of a time step being part of a blocking event that lasted a minimum of 5 days, for the 30 year period separated by year and/or season. Probability is obtained with the logistic regression models using the season $\text{Seas} \in \{\text{DJF}, \text{MAM}, \text{JJA}, \text{SON}\}$ as a categorical term in the predictor

$$\text{logit}(p) \sim \text{Year}, \tag{19}$$

$$\text{logit}(p) \sim \text{Year} * \text{Seas}. \tag{20}$$

where the months December, January, February, etc. have been abbreviated by capital letters D, J, F, and so forth. In the following, we test parameter estimates being different from zero using the z-test with p-values encoded as

$$0 < (^{***}) < 0.001 < (^{**}) < 0.01 < (^{*}) < 0.5. \tag{21}$$

The black lines in Fig. 7 show the probabilities for the full year (Eq. 19) and the colored lines show the development of the blocking probability in the individual seasons using a model with interactions (Eq. 20). Within the study period, the annual blocking probability (black line) increases significantly(**) in the whole domain (Fig. 7a) and also significantly(*) in the Euro-Atlantic region (Fig. 7b). However, these increases are rather small by two, and one percent points, respectively. The average probability is about 25% blocked time steps in $90° W$ to $90° E$ and about 15% blocked time steps in $40° W$ to $30° E$. his is in accordance with the fraction of blocked time steps per year plotted in Fig. 6a,b.

Using season as interaction effect in the regression (Eq. 20) reveals that this increase over the 30 years stems to a large extend from a significant increase of probability of blocked time steps in the summer months (JJA)(***) from $p \approx 0.17$ to $p \approx 0.27$ in $90° W$ to $90° E$ (Fig. 7a). Furthermore, in the larger domain the probability of blocked time steps in winter (DJF)(***) increases significantly, too, while the probability decreases in spring (MAM)(*) and autumn (SON)(***) (Fig. 7a).
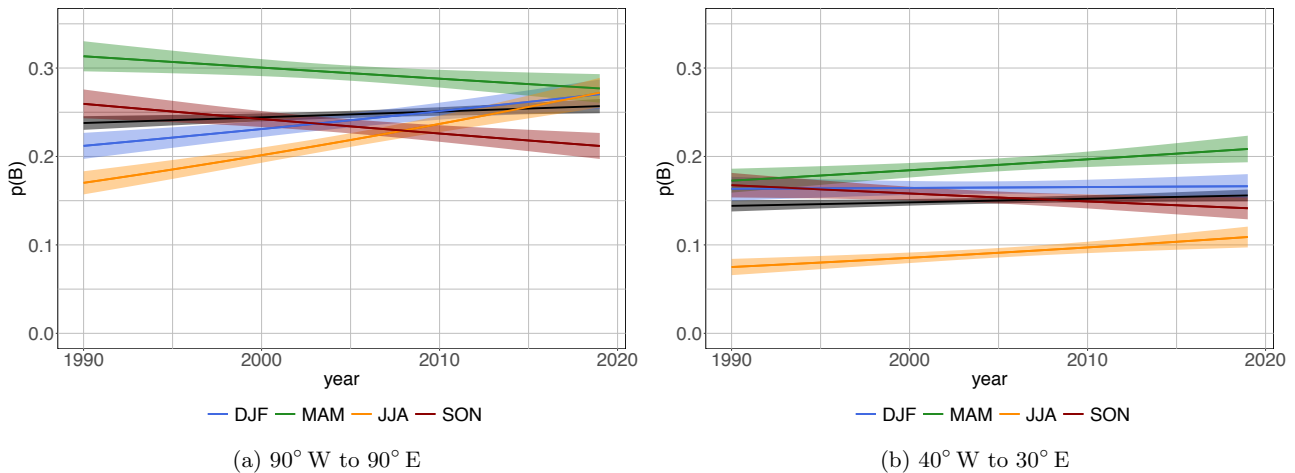
Figure 7. Blocking probability over time for the full *year* (black line, Eq.19) and for individual *seasons* (colored lines, Eq. 20). Shadings shows 95% confidence intervals. (a) $90° W$ to $90° E$ and (b) selected Euro-Atlantic region ($40° W$ to $30° E$).

In contrast to the decreasing probability observed for the spring season in the larger region (Fig. 7a, green line), we observe
395   a significant increase in spring (MAM)(***) in the Euro-Atlantic sector (Fig. 7b, green line). The probability of blocking increases significantly in summer (JJA)(***), too, although summer yields the lowest probability of all seasons in the Euro-Atlantic region (Fig. 7b, yellow line). Moreover, 7 out of the 11 experiments show this significant increases in spring and summer. Autumn and winter show no significant trends in the Euro-Atlantic sector.

4.2.2 Monthly blocking probability in the Euro-Atlantic region

400   With a categorical term for the month $\text{Mon} \in \{1, 2, 3, \ldots, 12\}$ in the predictor, interacting with Year

$$\text{logit}(p) \sim \text{Year} * \text{Mon}, \tag{22}$$

we have more temporal detail and can pinpoint the drivers of the observed trends in blocking probability in the Euro-Atlantic sector down to specific months (see Fig. 8).

All summer months, especially June and August, show a slight, but steady increase of blocking probability (see Fig. 8c, not
405   significant) and contribute likewise to the observed general increase in summer (Fig. 7 right, yellow-orange line). Similarly, the general decrease of blocking observed in autumn (SON) is mirrored in all months, too, especially in September and October (Fig. 8d,(*)). On the other hand, the the winter and spring seasons show more disagreements. For example, we observe an increase in Spring (MAM) on a seasonal basis. This increase can mainly be attributed to a strong significant increase of blocked time steps in March(***) from about 10% blocked time steps in 1990 to about 25% in 2019. While April is relatively
410   stable over the whole period, we observe a significant decrease of blocked time steps for May(**). However, this decrease is smaller in magnitude from about 20% to about 15% than the increase in March. The winter months (DJF) show no clear trend
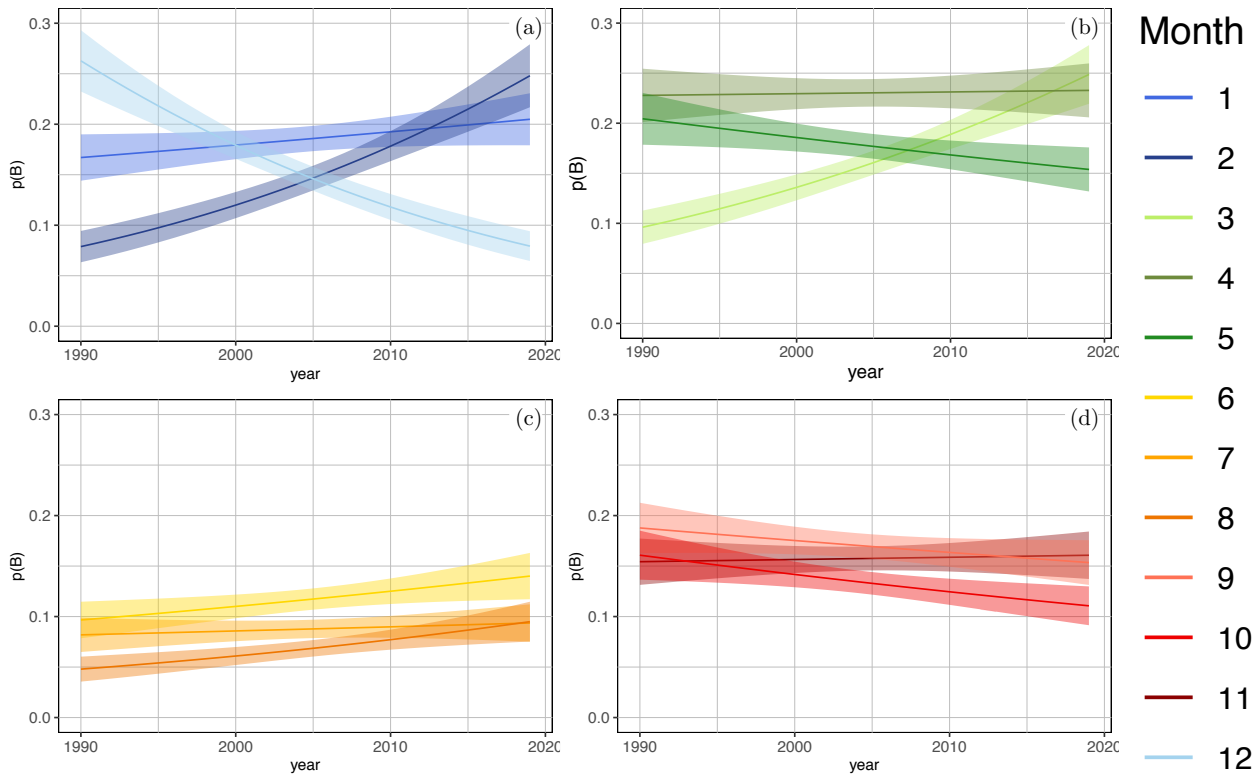
Figure 8. Blocking probability over time for individual month (Eq. 22). Shadings show 95 % confidence intervals. (a) winter (DJF) (b) spring (MAM) (c) summer (JJA) and (d) autumn (SON) in the Euro-Atlantic region ($40° W - 30° E$).

over the 30-year period on a seasonal basis (Fig. 7a, blue line). But the single months show a different behaviour (Fig. 8a): While blocked time steps in December(***) decrease significantly, the probability for blocked time steps in February increases strongly (***) for the same period. Moreover, all experiments with different distance criteria agree on the significant decrease in December and the significant increases in February, March and August. A significant decrease in October is only observed for the 6 experiments with the strictest distance criteria.

4.3 Temporal development of blocking probabilities – Three-states blocking model

In the following, we additionally distinguish between the two blocking types *High-over-Low* and *Omega* blocks using the three-states model.

(a) 90° W to 90° E   (b) 40° W to 30° E
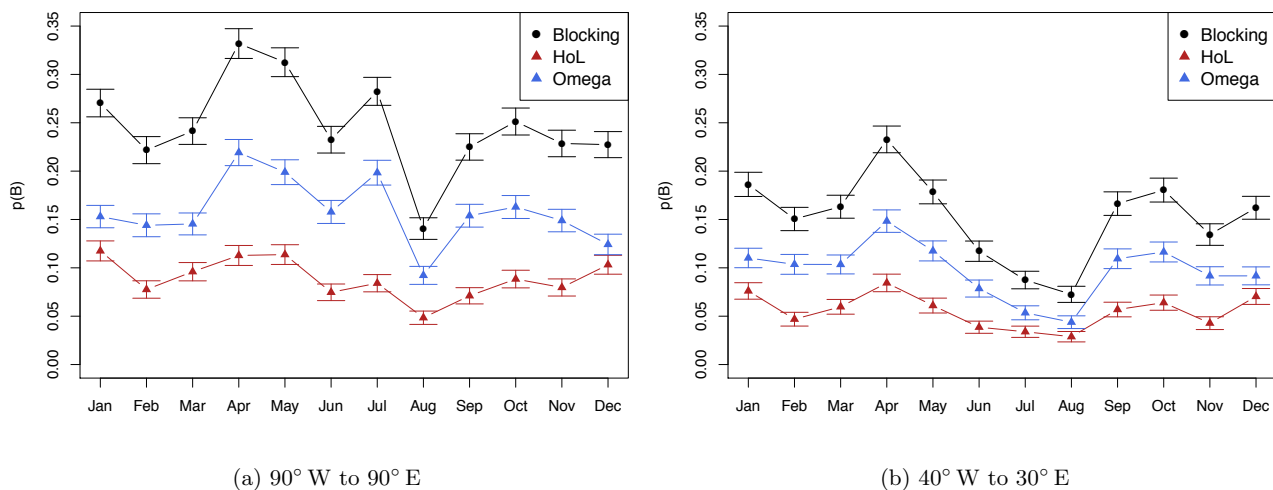
Figure 9. Blocking probability estimated for individual months for blocking in general, as well as separately for *High-over-Low* and *Omega*. (a) whole domain (90° W to 90° E) and (b) Euro-Atlantic subsection (40° W to 30° E). Whiskers shows 95% confidence intervals assuming Gaussian asymptotic for estimating binomial probabilities.

4.3.1 The annual cycle of blocking probability

Taking a look at the annual cycle of blocking probability reveals that the colder months from September to March are characterized by relatively high, but stable blocking probabilities of about 22% ($\approx$ 15%) in 90° W to 90° E (40° W to 30° E) with a smaller peak in January (see Fig. 9). The main peak in both regions occurs in April. While the larger region (90° W to 90° E) shows a broader peak with high values in May and a secondary peak in July, in the Euro-Atlantic region the blocking probability only peaks in April and shows a broader minimum in June to August. In the larger region, the lowest blocking probability occurs in August, too, but June and July have higher probabilities. In general, About 2/3 of the blocked time steps can be classified as *Omega* blocks and about 1/3 as *High-over-Low* blocks. Only in December and January, this classification rather changes to about 1/2 (both regions, red/blue triangles in Fig. 9). It should be noted that a blocking does not have to occur in every month of every year (see Supplementary Material Fig. S.6 and Fig. S.7). Further differences can be seen for the two types of blocking. For *Omega* blocks, greater fluctuations can be seen within the individual years (see Supplementary Material Fig. S.6 and Fig. S.7 for more details). At this point it should also be pointed out that it is possible that only a few time steps of a blocking lie in one month while the other time steps are in an adjacent month.

4.3.2 Seasonal and monthly blocking probability in the Euro-Atlantic sector

The three-state blocking model with distinct *High-over-Low* and *Omega* blocks can be described in a similar manner as the two-state Markov model but using multinomial logistic regression (Sec.3.5) with reference $Pr\{Y_t = nB|Y_{t-1}\}$. The models

(a) High-over-Low blocking, $40°$ W to $30°$ E

(b) Omega blocking, $40°$ W to $30°$ E
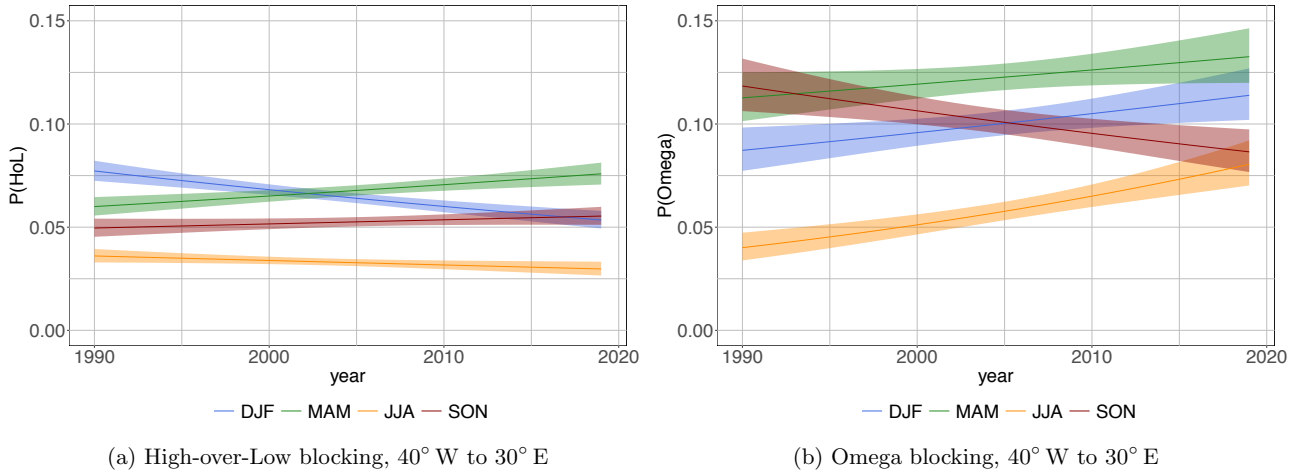
Figure 10. Temporal development for individual seasons (Eq. 23) for the blocking probabilities for the Euro-Atlantic region ($40° W - 30° E$) for (a) *High-over-Low* and (b) *Omega* blocking.

used here are

$$\ln\left(\frac{Pr\{Y_t = HoL\}}{Pr\{Y_t = nB\}}\right) \sim \text{Year} * \text{Seas}, \qquad \ln\left(\frac{Pr\{Y_t = \Omega\}}{Pr\{Y_t = nB\}}\right) \sim \text{Year} * \text{Seas}, \qquad (23)$$

$$\ln\left(\frac{Pr\{Y_t = HoL\}}{Pr\{Y_t = nB\}}\right) \sim \text{Year} * \text{Mon}, \qquad \ln\left(\frac{Pr\{Y_t = \Omega\}}{Pr\{Y_t = nB\}}\right) \sim \text{Year} * \text{Mon}. \qquad (24)$$

As described in Sec. 3.5, for both cases, the seasonal and the monthly case, we need two equations, one for $Pr\{Y_t = HoL\}$ and one for $Pr\{Y_t = \Omega\}$.

Figure 10 shows the temporal evolution of the probabilities of the two blocking types broken down to the seasons. The probability of *High-over-Low* blocks in the Euro-Atlantic region shows a decrease/slight decrease in winter (DJF)/summer (JJA,(**)) and an increase/slight increase in spring (MAM,(*))/autumn (SON,(*)) over the 30-year period (see Fig. 10a)[3]. At the same time, the probability for *Omega* blocks increases strongly in the summer months (***) and also pronounced in winter(**) and spring (see Fig. 10b). Only the *Omega* blocks in autumn (SON,(**)) decrease over the 30 years[4]. Interestingly, the blocked summer *High-over-Low*s start with the same probability as the *Omega* blocks in the 1990s. However, while the probability increases strongly for *Omega* blocks, it shows only a very slight increase for *High-over-Low*s. Hence, the observed, general increase in summer blocking probability (Fig. 7b) can be attributed to an increase in *Omega* block patterns. This increase occurs in all three summer months, but stronger in June and August (see Fig. 8c).

---

[3]All 11 experiments agree on the decrease of *High-over-Low* probabilities in DJF and 9 out of 11 experiment show the significant increase in SON.

[4]For the *Omega* blocks 10 out of 11 (8 out of 11) experiments agree on the significant increase in JJA (DJF). All experiment agree on a decrease in SON, but only 5 of them are significant.
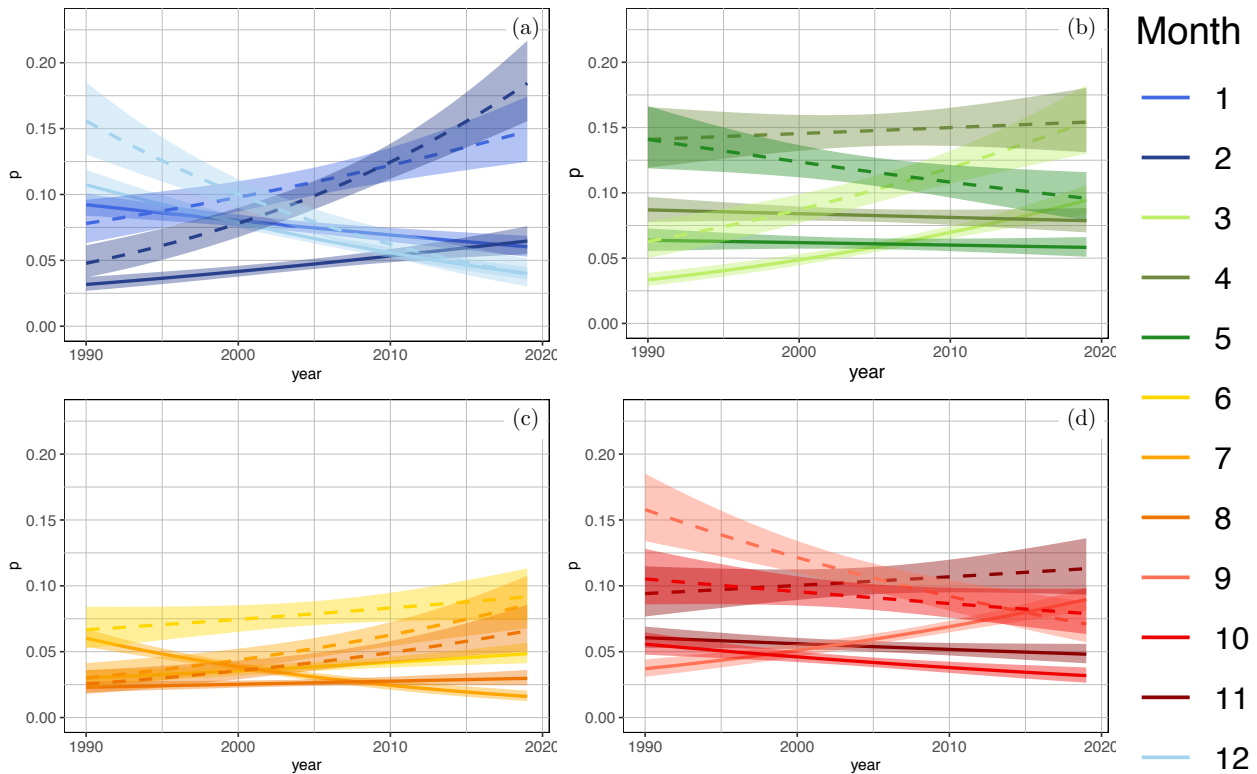
Figure 11. Blocking probability over time for individual month (Eq. 24) for *High-over-Low* (solid) and *Omega* (dashed) blocking. Shadings show 95% confidence intervals. (a) winter (DJF) (b) spring (MAM) (c) summer (JJA) and (d) autumn (SON) in the Euro-Atlantic region ($40° W - 30° E$).

450   A refinement based on monthly resolution is shown in Fig. 11. In the winter season, we observe an increase of *Omega* blocks in February and January and a decrease in December (Fig. 11a, dashed lines). The *High-over-Low* blocking decrease in December and January and only slightly increase in February (see Fig. 11a) December and January are significant (***) for both blocking types, February is only significant for *High-over-Low*s (**). In spring, the probabilities for *High-over-Low* blocking remain more or less constant, with only a slight increase in March. *Omega* b   therefore play a greater role in the

455   development of these frequencies here as well. The highest change is in March(***) and a decrease in May(***) (see Fig. 11b). In the summer months the change is not as pronounced than in the other seasons and is again mainly dominated by *Omega* blocks (see Fig. 11c,not significant). In autumn there is no significant trend in the blocking probability of the two-state model (see Fig. 7b). An analysis of the individual months shows a slight increase in the probabilities in November for *Omega* blocks (not significant) and a decrease for *High-over-Low*s(***). The other two months, however, show a decrease for *Omega* blocks.
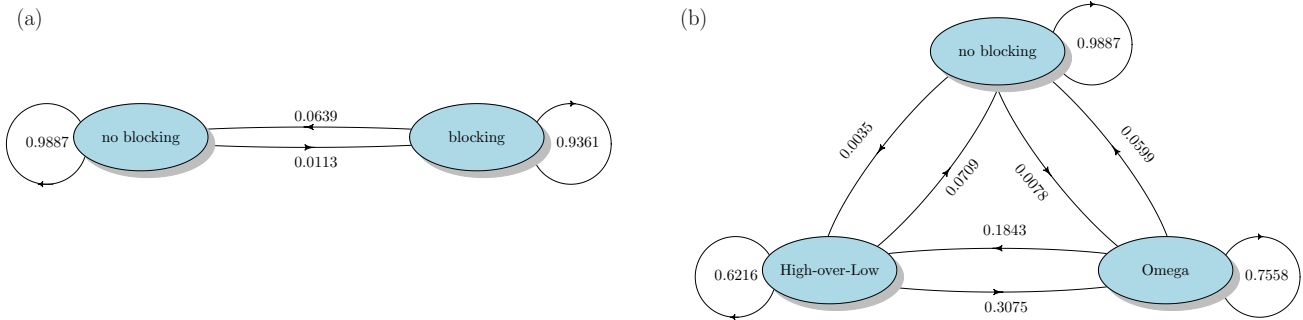
Figure 12. Graph representation of transition probabilities of the transition matrix estimated for a Markov process (a) with two states (Eq. 14) and (b) with three states (Eq. 15) in the Euro-Atlantic region ($40° W - 30° E$).

460 For *High-over-Low* blocks a slight increase is shown for September and a decrease in October. All in all, this balances itself out.

4.4 Transition probabilities

We conceive the dynamics between different blocking and no-blocking states as a stochastic process with Markov proper-ties (see Section 3.6) and give transition probabilities for the two- and three-states model with stationary and non-stationary 465 assumptions in the following.

4.4.1 Transition probabilities of two- and of three-state models

Assuming stationary transition probabilities, we can estimate transition matrices for the two- and of three-state models. Fig-ure 12 shows the transition probabilities of the two-state Markov model with *no blocking* and *blocking* (Fig. 12a) and the three-state Markov model with the states *no blocking*, *High-over-Low* and *Omega block* (Fig. 12b). We call the probability to 470 remain in one state *stability* or *persistence* and the transition from *no blocking* to a *blocking* (*High-over-Low* or *Omega*) *onset* which indicates the formation of a blocking; the opposite direction is called *offset* which can also be seen as a decay. In this work we will stick with the terms *onset* and *offset* as we focus on the model view, in which there is only the state "on" or "off". From a meteorological point of view, the use of the word "decay" describes the transformation from a blocked state to an unblocked state with the right words, as it is a process. For both models, persistence (probability to remain in one state) of 475 either state is higher than transition probabilities to other states; particularly high is the persistence of the no-blocking state. The latter is due to the fact that there are considerably more time steps without blocking than blocked states. But if blocking occurs, the probability to remain in this condition is high, too.

For the three-states model, the onset probability for an *Omega* blocking is higher than that for a *High-over-Low* blocking. Both values are small compared to the persistence defined above. This is consistent with the fact that onsets are less fre-480 quent. With this model, we obtain that *Omega* blocking is more stable than *High-over-Low* blocking, i.e. $Pr\{Y_t = \Omega \mid Y_{t-1} = $

$\Omega\} > Pr\{Y_t = HoL \mid Y_{t-1} = HoL\}$. Moreover, a *High-over-Low* block evolves more likely into an *Omega* block than vice versa. This means that another low-pressure system disturbs the *High-over-Low* block and the structure changes to an *Omega* blocking. This occurs more often than that a low pressure system leaves the *Omega* block and thus turns the system into a *High-over-Low* pattern. The offset (or decay) of an *Omega* block to the unblocked state is also less likely than the decay of a *High-over-Low* block, i.e. $Pr\{Y_t = nB \mid Y_{t-1} = \Omega\} > Pr\{nB \mid Y_{t-1} = HoL\}$.

4.4.2 Trends of transition probabilities of two- and of three-state models

Of particular interest is a potential change in transition probabilities during the study period 1990 to 2019. For this purpose, we describe the change in transition probabilities using logistic and multinomial regression with year (and season) as interacting terms in the predictor. For the two-state Markov model no significant changes neither with year as given in Eq. 16 (see Supplementary Material Fig. S.8) nor with interacting terms for year and season

$$\text{logit}(Pr\{Y_t = B \mid Y_{t-1}\}) \sim Y_{t-1} * \text{Year} * \text{Seas}, \tag{25}$$

(see Supplementary Material Fig. S.9) are identified. Breaking this down to a three-state Markov model we get the following equation for yearly changes

$$\ln\left(\frac{Pr\{Y_t = HoL\} \mid Pr\{Y_{t-1}\}}{Pr\{Y_t = nB \mid Y_{t-1}\}}\right) \sim Y_{t-1} * \text{Year}, \qquad \ln\left(\frac{Pr\{Y_t = \Omega\} \mid Pr\{Y_{t-1}\}}{Pr\{Y_t = nB \mid Y_{t-1}\}}\right) \sim Y_{t-1} * \text{Year} \tag{26}$$

and Eq. 17 and 18 (see also Sec. 3.6) for the trends with interacting terms for year and season. Figure 13 shows the temporally varying transition probabilities for the three-state model arranged analogously to the transition matrix (Eq. 15). The shadings give 95% confidence intervals.

Similar to the tendency we see in the two-state model, the probability for remaining in an unblocked state (Fig. 13a) slightly decreases and the onset probability of *Omega* blocks (Fig. 13c) slightly increases. For the three-state Markov model, these trends are significant[5]. Note also the decrease of transition probability from *Omega* to *High-over-Low* $p_{HoL|\Omega}$ (Fig. 13h[6]) which is compensated by an increase in persistence of *Omega* $p_{\Omega|\Omega}$ (Fig. 13i) and an increase of offset probability from *Omega* blocking $p_{nB|\Omega}$ (Fig. 13g) (all three not significant). We can thus refine the impression from the two-state model: blocking are more frequent and those are predominantly *Omega*, which become more stable and do less likely evolve into *High-over-Low*s.

Breaking this down into seasons by adding another interaction effect (Eq. 17 and Eq. 18), we obtain Fig. 14. The largest temporal changes can again be observed in the summer months. The first row shows an increase in the onset probability for *Omega* (Fig.14c) blocks in summer while the probability of remaining in a no blocking state (Fig.14a) decreases (both significant,*). The last row shows that *Omega* blocks (Fig.14i) become slightly more stable in summer towards the end of the study period and becomes less likely to evolve into a *High-over-Low* (Fig.14h) (both not significant). Changes in transition probabilities for *High-over-Low* blocks are in the second row of Fig.14: A decrease in persistence in summer and an increase in

---

[5]All experiments agree on the decrease in persistence of the unblocked state (8 out of 11 show a significant decrease) and all agree on the increase of the onset probability of the *Omega* blocks (6 out of 11 significantly)

[6]6 out of 11 experiments show a significant decrease of the transition probability from *Omega* to *High-over-Low*, all agree on the decrease however.
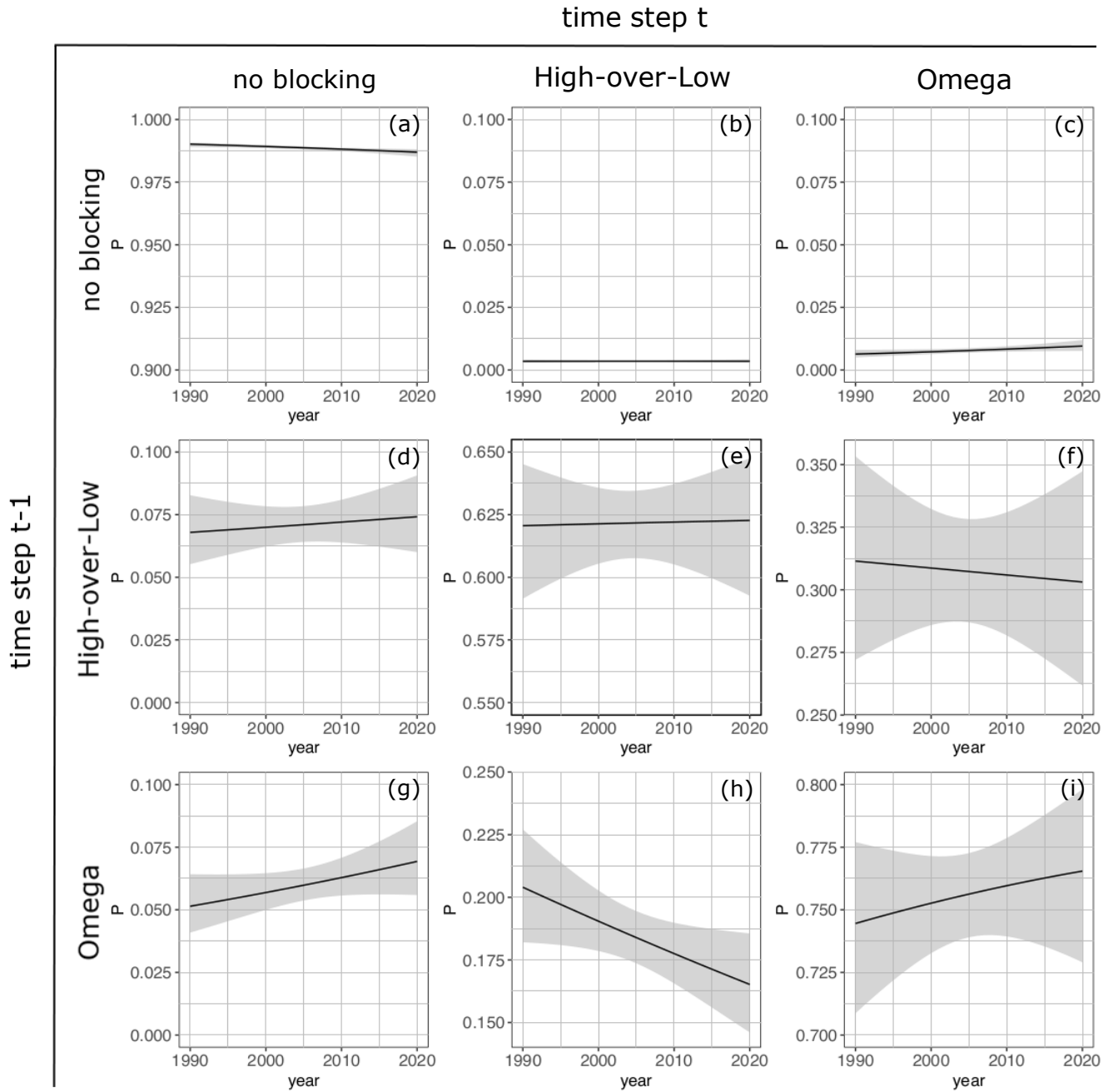
Figure 13. Transition probabilities analogous to the matrix of a three-state Markov process (Eq. 15) as a function of years (Eq. 26) in the Euro-Atlantic region ($40° W - 30° E$). (a) $p_{nB|nB}$, (b) $p_{HoL|nB}$ (c) $p_{\Omega|nB}$, (d) $p_{nB|HoL}$, (e) $p_{HoL|HoL}$ (f) $p_{\Omega|HoL}$, (g) $p_{nB|\Omega}$, (h) $p_{HoL|\Omega}$ and (i) $p_{\Omega|\Omega}$. Shadings show 95 % confidence intervals.
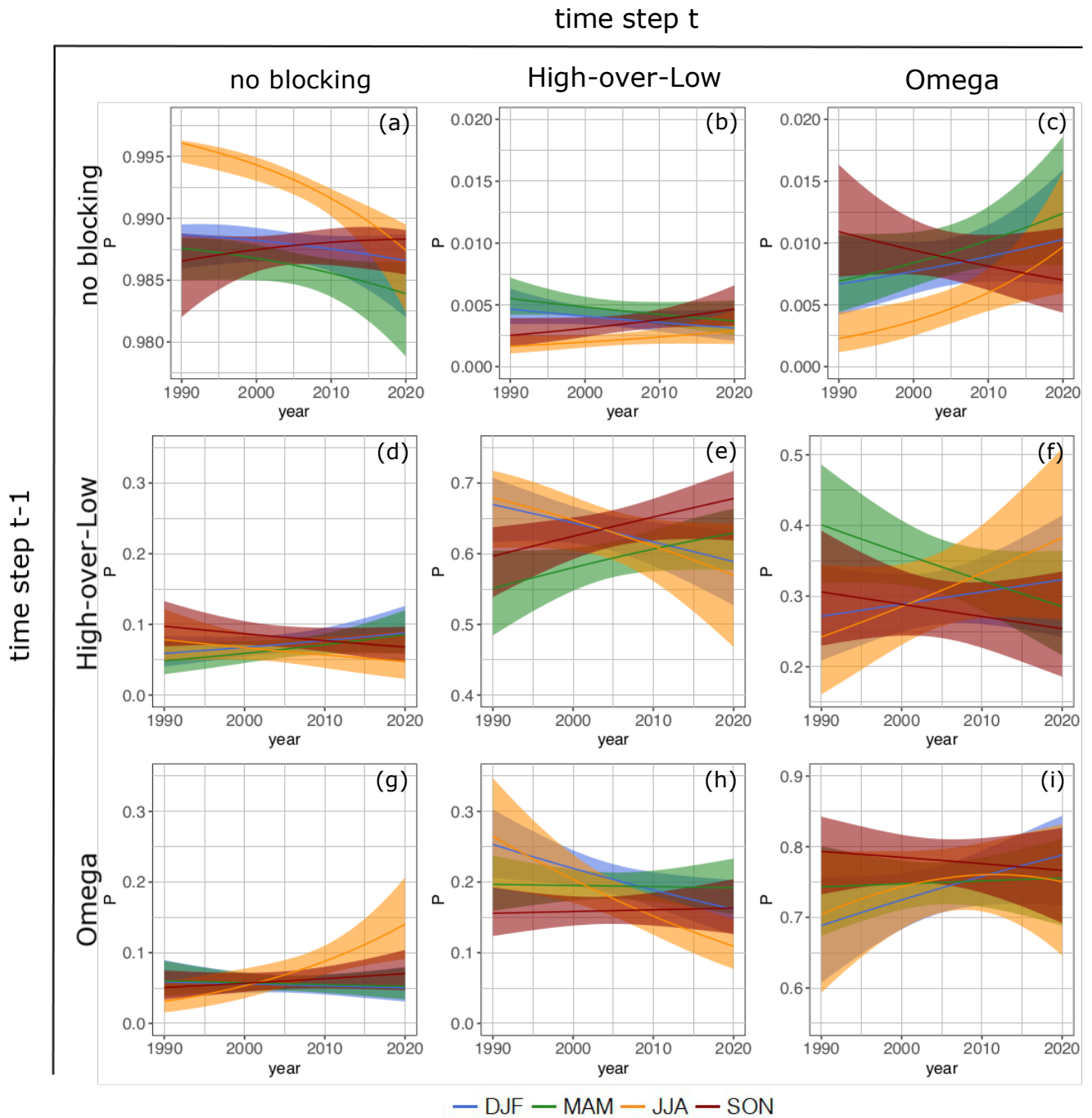
Figure 14. Transition probabilities analogous to the matrix of a three-state Markov process (Eq. 15) as a function of years for individual seasons (Eq. 17 and Eq. 18) in the Euro-Atlantic region ($40°\,W - 30°\,E$). Panels are ordered analogously to Fig. 13, season is color coded. Shadings show 95 % confidence intervals.

stability in the other seasons (Fig.14e) (all not significant). The transition probabilities towards *Omega* blocks (Fig.14f) increase strongly in summer and slightly in winter and decrease in the transition seasons (all not significant). Although not significant, this confirms again the previously gained impressions: *Omega* blocks become more frequent and stable in summer and the transition probability of *High-over-Low* to *Omega* decreases in summer. The persistence of *High-over-Low*s increases over the years in the transition seasons and become less likely to evolve into an *Omega*, although these changes are not significant.

5   Discussion

In this work, we analyse atmospheric blocking probabilities in general and the onset, offset and transition probabilities of blocking in particular. Moreover using a novel method based on the kinematic vorticity number and point vortex theory, we are able to identify and distinguish between two different blocking types: *High-over-Low* and *Omega* blocking. The location of the low-pressure areas is of general importance, as the two different blocking types can affect and impact different regions due to their different structures. Using the novel method we can affirm the first question from the introduction, if we can find a method to automatically distinguish between the two different atmospheric blocking types.

In order to estimate the uncertainties of the method, we did a number of experiments depending on different distance criteria for the maximum distance between circulation centroids of successive time steps. The number of identified blocks is sensitive with respect to the distance criterion with lower number for stricter criteria. However, the majority of the experiments agree on the significant results we observe. The main intention to use such a distance criterion is that we want to investigate blocking as a Lagrangian system that we follow in time. The high is assumed to be the same vortex over the whole lifetime, but we allow for local variations in and replacements of the low(s). This distinguishes our method and analysis from other studies that rather focus on blocking as a large-scale weather regime within a defined region (Eulerian perspective).

As second question, we asked about the occurrence of the different blocking types and if they undergo long-term changes. We further asked if there is a seasonal or even monthly dependence for the different blocking types. By evaluating the occurrence probabilities of the different blocking types we find that the probability of the occurrence of an *Omega* blocking is higher than that of a *High-over-Low*, see Fig. 9. In the Euro-Atlantic region, the majority of blocks occur in the transitional seasons spring, autumn and in winter for both blocking types (Figs. 9b, 10, 11). However, their trends are partly contrary: For example we see significant increases of *Omega* probabilities in summer and winter, but a decrease in autumn in the 30-year period. On the other hand, the probability of *High-over-Low* blocks decreases significantly in winter and summer and increase in autumn (Fig. 10). We can refine this results considering months: While in July *Omega* blocks account for only about 25% of all observed blocks in 1990, we find on the one hand an increase in the number of blocks in general as well as a higher fraction of *Omega* blocks towards the end of the study period. In 2019, the *Omega* blocks pose about 80% of all blocking. Interestingly this relation is reversed in September where the *High-over-Low*s constitute about 20% of all blocking in 1990 vs. about 55% in 2019. It is not clear, why there is a change in the distribution of blocking types. Future studies are challenged to look for changes in e.g. dynamical processes in this time period that might cause these differences.

In summer, especially in August, the probability of blocking is the smallest. This can be explained by the variation of the pressure anomalies. In spring and autumn the amplitudes of the pressure anomalies are larger than in summer (see, e.g. Wallace et al., 1993). Therefore, the high and low pressure systems are more distinct and can last longer. In Fig. 7b the

545 blocking occurrence probabilities split to seasons are illustrated, where the low probability of blocking in the summer months in the Euro-Atlantic sector is clearly recognizable. Tyrlis and Hoskins (2008) and Brunner et al. (2017) show similar results regarding the blocking minimum in summer. But as shown in Fig. 7b the probabilities of blocks slightly, but significantly increase in summer. Therefore, occurrences of exceptional droughts, that were experienced 2018 and 2019 in central Europe (Hari et al., 2020) could occur more often in the future.

550 Furthermore, over the 30 year period we observe a strong increase of blocked periods in February and March (Fig. 8). These late winter/early spring blocks can have a significant impact on the vegetation and on agriculture in general since they are often connected to temperature extremes. For example, Brunner et al. (2017) found a strong link between cold spell days in February and co-occurrence of blocking, and a link between warm spell days and blocking in late spring in Europe, but they found *no apparent trend in the number of blocked days*. However, their study focus laid on temperature extremes and not on

555 blocking trends and their identification method differed from ours. In their work on observed blocking trends during the time period 1980–2012, Barnes et al. (2014) did not find a *clear hemispheric increase in blocking* that *is evident in any season for any blocking index, although robust seasonal increases and decreases are found for isolated regions.* We can partly confirm this statement: although we find significant trends regarding the seasons, these trends are small and depend on the region. For example the general increase in summer in the Euro-Atlantic region is only in the order of 4 percent points. While spring blocks

560 increase in the Euro-Atlantic region, they decrease in the larger region from $90°W$ to $90°E$. However, adding more detail to the analysis by considering blocking types and months leads to significant and stronger trends in some months. However, it should be kept in mind that this further division of the data set leads to smaller sample.

Fig. 12b shows that *Omega* blocks are more persistent than *High-over-Low* blocks. Furthermore, the formation or onset probability of an *Omega* block is higher than that of a *High-over-Low* blocking. And the transition probability from the *High-*

565 *over-Low* state to the *Omega* block is 0.3, whereas the transition probability from a *High-over-Low* to an *Omega* block is considerably smaller (0.18). Analysing composites of the blocking onset in the time period June to August, Drouard and Woollings (2018) found that Western- and Central Europe are dominated by a *High-over-Low* pattern while they found dominating *Omega* pattern for East Europe east of $35°E$. In order to compare their results with our work, we plotted the total number of blocked time steps with respect to the blocking types and longitudes of occurrence in Fig. 15. In general, we observe more

570 *Omega* blocks (about 2/3) than *High-over-Low*s (about 1/3). However, we observe that the share of *High-over-Low*s in the total number of blocked time steps is highest between about $0° - 40°E$ and between about $60°E - 75°E$. The fraction of *Omega* blocks is highest for longitudes west of $25°W$ and for a the region between about $40°E - 60°E$. This is comparable to the results of Drouard and Wollings (2018) for their regions between $0°$-$55°$. Their composites for the areas of Western-south central Europe (0–$20°E$, 40–$50°N$); Central Europe (20–$40°E$, 50–$60°N$) and Western Russia (35–$55°E$,45-$55°N$) indeed showed rather

575 *High-over-Low* patterns for the first two regions and an *Omega* pattern for Western Russia. However, our analysis in Fig. 15 is based on the whole year, while Drouard and Woollings (2018) looked at the summer months June to August.
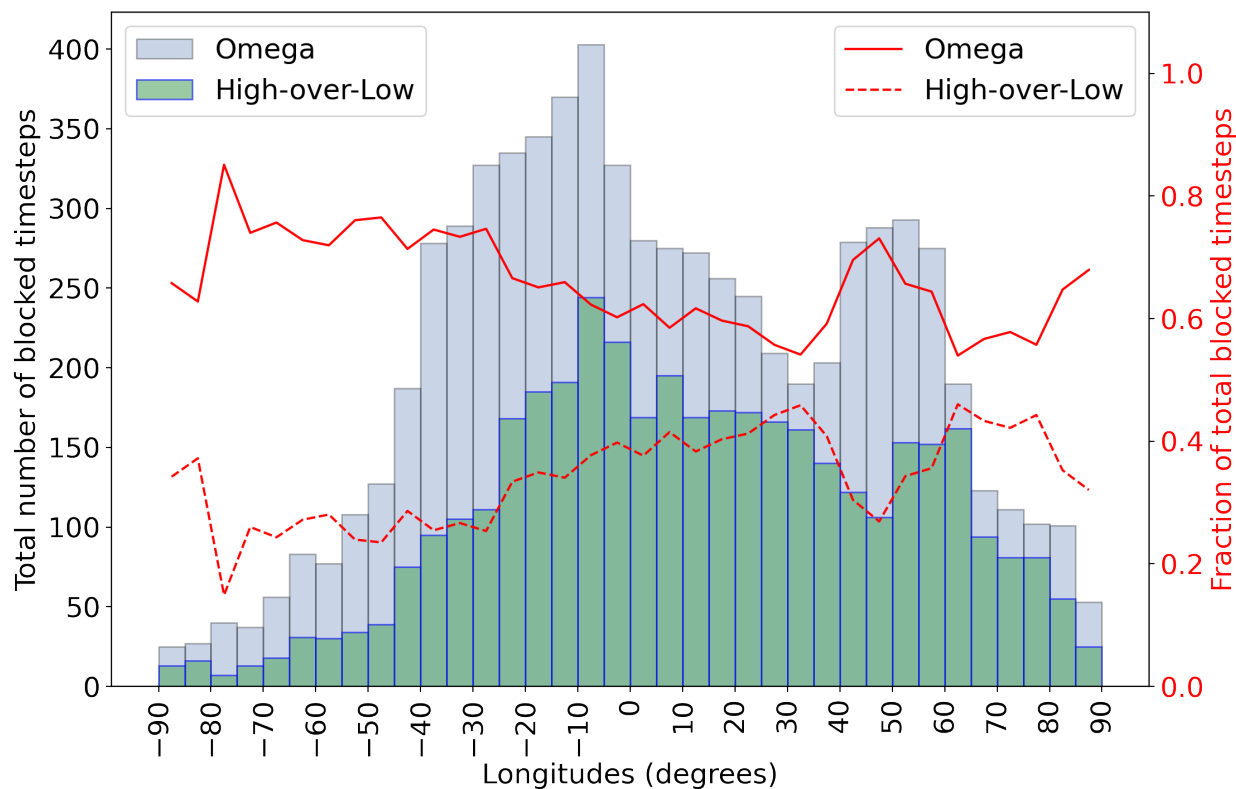
Figure 15. Number of total blocked time steps for *Omega* and *High-over-Low* blocks (columns) and percentage of *Omega* (solid red line)/*High-over-Low* (dashed red line) blocks with respect to total blocked time steps. Note that this analysis is based on all blocked time steps in the period 1990-2019. No distinction has been made between season or onset/offset.

The general transition of the two states *no blocking* and *blocking* in Fig. 12a shows that the probability of a block remaining blocked for the next 6 hours is 0.94. The probability of the onset, i.e. the transition probability from the state *no blocking* to the state *blocking*, is much lower (about 1%) than the offset probability (about 6%), because there are more time steps unblocked than blocked. In comparison, Spekat et al. (1983) found daily transition probabilities for the onset of a meridional weather regime of 8% (zonal→meridional) to 11% (mixed state→meridional) and high probabilities to stay within the same weather regime (between 0.81 and 0.86). Their offset probabilities range from 5% (meridional→zonal) to 9% (meridional→mixed state). Their onset values are comparable to our results if we downscale the 6-hourly data to daily time steps. Moreover, we can confirm that the probability is higher to remain within the same state. A more detailed comparison is complicated, because their method differs from the one we use. While Spekat et al. (1983) uses a large-scale weather regime classification, our method is based on the identification of the blocking pattern itself and is rather event-based.

Finally, we tackle the third question asked in the introduction: Are there trends in the transition of different blocking types and do these transitions depend on the season, or even on the month? The results of the transitions for the two-state model and the three-state model does not show significant trends on a yearly analysis (see Supplementary Material Fig. S.8 and Fig. 13). But the further split into the seasonal temporal evolution shows a significant trend of the onset and offset of *Omega* blocks during the summer months, see Fig. 14c,g. The conversion from an *Omega* block to a *High-over-Low* decreases (Fig. 14h). Lucarini et al. (2016) finds that blocking periods are characterized by higher instability than unblocked flows. This might also justify the occurrence of blocking type changes from *High-over-Low* to *Omega* and vice versa.

We remark that the outcomes depend on the methods and on the time resolution. Using data with a 6 hourly time resolution, we obtain a larger data basis compared to data based on daily means. Regarding the methods, the blocked time steps are initially identified with the help of the instantaneous blocked longitudes (IBL) method after Tibaldi and Molteni (1990), see also Peng et al. (2015). The identification algorithm (Step 1-4, Section 3, see also Fig. 2) is based on many assumptions and not flawless. The IBL method is a one-dimensional method. Although we applied a seasonally varying reference latitude, a one-dimensional method might have problems in detecting blocked situations properly. Especially, the thresholds of northern and southern geopotential height gradients are fixed values and applied for the whole year. This might explain why there are fewer blocks detected in summer. See also e.g. Scherrer et al. (2006), who show that the frequency of blocks is strongly dependent on the reference latitude. Moreover, the choice of the investigated domain can have an impact on the results, see e.g. Fig. 7. We also note that the data assimilation techniques as well as the amount of observational data assimilated did change over the years, which can lead to slightly inhomogeneous data. This might further obscure real trends from artificial ones (Sterl, 2004). Since our study regions are in the northern hemispheric mid-latitudes and our period lies in the post-satellite era, we expect the data to be relative homogeneous. We also choose five days (=20 time steps) as a minimum duration for our definition of blocking in the larger domain. Although we made a subset of the larger domain and the length of stay within the smaller Euro-Atlantic sector can be smaller than 5 days, the minimum lifetime of the associated block period is still 5 days. However, changing this minimum duration criterion leads to a higher or lower number of identified blocks. Investigating the blocking identification methods based on the vertically averaged potential vorticity anomaly (Schwierz et al., 2004), the geopotential height anomaly (Dole and Gordon, 1983), and geopotential height gradient after Tibaldi and Molteni (1990) that is applied here, Pinheiro et al. (2019) found that *each of these algorithms produce distinct regional and seasonal differences in their overall global blocking climatology*. Moreover, the decision between *High-over-Low* and *Omega* blocking types is based on a comparison of the vortex field south of the high center. The vortex field is inspected in a box with a width of 25 degrees longitudes directly below the high and compared to the two neighboring boxes (see Fig. 3). A change in the box width obviously can affect the percentage of identified *High-over-Low*s vs. *Omega* blocks. In our setting, the method identifies about 2/3 of all blocking as *Omega* types. However, this changes the ratio of identified *Omega* vs. *High-over-Low* blocks, but does not explain the partially contrary trends in their probability in some months such as the increase of *Omega* blocks in summer while the *High-over-Low*s decrease. These must stem from another mechanism, maybe a change in the underlying large-scale flow or the position or strength of the jet. Furthermore, changing the region of interest (Step 4 in Section 3) can lead to different results than previous works. A major benefit of this approach based on the kinematic vorticity number is the identification and location of each

single vortex – the high pressure area as well as the one or two low pressure areas – forming the *High-over-Low*, respectively the *Omega* block.

6 Conclusion

Using logistic regression and the Markov model, we investigate onset, offset and transition probabilities of atmospheric blocking during the time period 1990-2019 in the Euro-Atlantic sector (40°W-30°E) and for the larger region (90°W-90°E). In the following, we will summarize our main results with respect to the three research questions posed in the introduction:

(1) Can we find a method to automatically distinguish between the two atmospheric blocking types *High-over-Low* and *Omega* blocks?

To tackle this first question, we introduced a blocking type decision method based on the kinematic vorticity number and point vortex principles, that identifies *High-over-Low* and *Omega* patterns for each blocked time step, separately. Blocked weather situations are usually analysed with respect to the persistent high, which can for example lead to droughts with devastating consequences. Using the point vortex theory, we require the sum of the circulations of the high and low pressure areas to be zero. The additional consideration of the low(s) in a blocking identification method is a novelty and provides the possibilities for further studies for example on the impact of the steady low pressure systems such as heavy rainfall and floods. In general, we observe that about 2/3 of all blocks are *Omega* blocks and about 1/3 are *High-over-Low* blocks, although this fractions can vary with longitude, season and year (Figs. 9, 15).
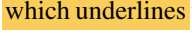
(2) Do blocking occurrence probabilities undergo long-term changes? Do these changes depend on the season or month?

For both regions, we observe only small significant changes in the yearly and seasonal blocking frequency over the 30 year period. But, we observe large significant increases in the blocking probability for some months, especially February and March. We observe a steady, but slight increase for the summer months, too.In addition, a strong significant decrease is observed in December over the 30 years. These changes can be attributed predominantly to *Omega* blocks (Figs. 7, 8, 10, 11).

(3) Do onset (formation), offset (decay) or transition probabilities from one blocking type to another undergo long-term changes? Do these changes depend on season or month?

In order to answer this third question, we use a Markov model to calculate transition probabilities of the different blocking types *High-over-Low* and *Omega* blocking and of the state *no blocking*. We show that *Omega* blocking is more likely to occur and more persistent than the *High-over-Low* blocking pattern (Fig. 12). Regarding the seasons over the 30 year period, we found the largest changes in transition probabilities in the summer season, where the transition probability to *Omega* blocks increase strongly, while the *unblocked* state becomes less probable. Hence, *Omega* blocks become more frequent and stable in summer. Moreover, we observe a higher probability for the transition from *High-over-Low* to *Omega* blocks in the summer season towards the end of the study period (cf. Fig. 14). This confirms the impression that blocking in summer become more

prominent in recent years over the European continents. Additionally, we show that this increase in summer blocking is explained by an increase in *Omega* blocking patterns.

655   In future studies, for a deeper understanding of atmospheric blocking, the relation of on- and offset of blocking to different parameters such as NAO, the temperature, or the wind shear should be investigated. Moreover, the authors suggest to either add a tracking method to the blocking identification process or substitute the blocking identification based on indices to a vortex identification method, for example based on the kinematic vorticity number (Schielicke et al., 2016). However, since the here introduced method can identify the high pressure area *and* the low pressure area, it can further be used for novel

660   statistical evaluations of extreme events caused by lows, as for example floods. Our results indicate rather monthly and more local changes of atmospheric blocks which underlines the necessity to analyse persistent high and low pressure areas separately. We conclude, that the use of logistic regression and the combination with Markov models with two and three possible states for different blocking types gives valuable insight into the development of atmospheric blocking especially when analysing the changes for seasons or individual months.

665   *Author contributions.* A.M., P.N. and H.R. designed the study. C.D. did the statistical analysis and visualised the results, mainly at the FU Berlin. L.S. wrote and adapted the trapezoid method and blocking type decision method and performed further uncertainty experiments. H.R. and C.D. wrote the statistical chapters and discussed the related results. C.D., A.M. and L.S. continuously wrote on the paper draft and discussed the results. All authors discussed and finalised together the paper.

Competing interests. The authors declare that no competing interests are present.

670   *Code and data availability.* The NCEP-DOE Reanalysis 2 data that supports the findings of this study is available via rda.ucar.edu with the identifier DOI:10.5065/KVQZ-YJ93. All code can be provided upon request.

Acknowledgements. We thank I. Kröner for critical discussions and reading the manuscript. This research has been partially funded by Deutsche Forschungsgemeinschaft (DFG) through grant CRC 1114 'Scaling Cascades in Complex Systems, Project Number 235221301, Projects A01 'Coupling a multiscale stochastic precipitation model to large scale atmospheric flow dynamics' and C06 'Multiscale structure

675   of atmospheric vortices'.

References

Altenhoff, A. M., Martius, O., Croci-Maspoli, M., Schwierz, C., and Davies, H. C.: Linkage of atmospheric blocks and synoptic-scale Rossby waves: a climatological analysis, Tellus A, 60, 1053–1063, https://doi.org/10.1111/j.1600-0870.2008.00354.x, 2008.

Aref, H.: Motion of three vortices, Physical Fluids, 22, 1979.

680 Baclawski, K.: Introduction to probability with R, Chapman & Hall/CRC Texts in statistical science, 2008.

Barnes, E. A., Slingo, J., and Woollings, T.: A methodology for the comparison of blocking climatologies across indices, models and climate scenarios, Clim. Dynam., 38, 2467–2481, https://doi.org/10.1007/s00382-011-1243-6, 2011.

Barnes, E. A., Dunn-Sigouin, E., Masato, G., and Woollings, T.: Exploring recent trends in Northern Hemisphere blocking, Geophys. Res. Lett., 41, 638–644, 2014.

685 Barriopedro, D., García-Herrera, R., Lupo, A. R., and Hernández, E.: A climatology of Northern Hemisphere blocking, J. Climate, 19, 1042–1063, https://doi.org/10.1175/JCLI3678.1, 2006.

Barriopedro, D., García-Herrera, R., and Trigo, R.: Application of blocking diagnosis methods to general circulation models. Part I: A novel detection scheme, Clim. Dynam., http://link.springer.com/article/10.1007/s00382-010-0767-5, 2010.

Berrisford, P., Hoskins, B. J., and Tyrlis, E.: Blocking and Rossby Wave Breaking on the Dynamical Tropopause in the Southern Hemisphere,
690 J. Atmos. Sci., 64, 2881–2898, https://doi.org/10.1175/JAS3984.1, 2007.

Bissolli, P., Deutschländer, T., Imbery, F., Haeseler, S., Lefebvre, C., Blahak, J., Fleckenstein, R., Breyer, J., Rocek, M., Kreienkamp, F., Rösner, S., and Schreiber, K.-J.: Hitzewelle Juli 2019 in Westeuropa – neuer nationaler Rekord in Deutschland, https://www.dwd.de/DE/leistungen/besondereereignisse/temperatur/20190801_hitzerekord_juli2019.pdf?__blob=publicationFile&v=3, Deutscher Wetterdienst, Abteilung Klimaüberwachung. Press release (in German), 1 Aug 2019 (last access: 31 Aug 2020), 2019.

695 Bott, A.: Synoptische Meteorologie, Springer Berlin Heidelberg, https://doi.org/10.1007/978-3-642-25122-1, 2012.

Brunner, L., Hegerl, G. C., and Steiner, A. K.: Connecting atmospheric blocking to European temperature extremes in spring, J. Climate, 30, 585–594, 2017.

Brunner, L., Schaller, N., Anstey, J., Sillmann, J., and Steiner, A. K.: Dependence of present and future European temperature extremes on the location of atmospheric blocking, Geophys. Res. Lett., 45, 6311–6320, 2018.

700 Cheung, H. N., Zhou, W., Mok, H. Y., Wu, M. C., and Shao, Y.: Revisiting the climatology of atmospheric blocking in the Northern Hemisphere, Adv. Atmos. Sci., 30, 397–410, 2013.

Davini, P. and D'Andrea, F.: From CMIP3 to CMIP6: Northern Hemisphere atmospheric blocking simulation in present and future climate, J. Climate, 33, 10 021–10 038, 2020.

Davini, P., Cagnazzo, C., Gualdi, S., and Navarra, A.: Bidimensional diagnostics, variability, and trends of Northern Hemisphere blocking,
705 J. Climate, 25, 6496–6509, 2012.

Deutscher Wetterdienst: The weather in Germany in July 2019, https://www.dwd.de/EN/press/press_release/EN/2019/20190730_the_weather_in_germany_in_july_2019.pdf?__blob=publicationFile&v=2, press release, 30 July 2019 (last access: 31 Aug 2020), 2019.

Deutscher Wetterdienst: DWD-Stationen Duisburg-Baerl und Tönisvorst jetzt Spitzenreiter mit 41,2 Grad Celsius, https://www.dwd.de/DE/presse/pressemitteilungen/DE/2020/20201217_annulierung_lingen_news.html, press release, 17 December 2020 (in German, last access:
710 11 Feb 2021), 2020.

Dobson, A. J. and Barnett, A. G.: An introduction to generalized linear models, Third Edition, Texts in Statistical Science, Chapman & Hall, 2008.

Dole, R. M. and Gordon, N. D.: Persistent anomalies of the extratropical northern hemisphere wintertime circulation: Geographical distribution and regional persistence characteristics, Mon. Weather Rev., 111, 1567–1586, 1983.

715 Drouard, M. and Woollings, T.: Contrasting mechanisms of summer blocking over western Eurasia, Geophys. Res. Lett., 45, 12–040, 2018.

Egger, J.: The blocking transition, in: Irreversible phenomena and dynamical systems analysis in geosciences, edited by Nicolis, C. and Nicolis, G., pp. 181–197, Springer Netherlands, Dordrecht, https://doi.org/10.1007/978-94-009-4778-8_10, 1987.

Ferranti, L., Corti, S., and Janousek, M.: Flow-dependent verification of the ECMWF ensemble over the Euro-Atlantic sector, Q. J. Roy. Meteor. Soc., 141, 916–924, 2015.

720 Freva: Freie Universität Berlin evaluation system (Freva), https://freva.met.fu-berlin.de/, accessed: 2020-09-10, 2017.

Gottwald, G. A., Crommelin, D. T., and Franzke, C. L. E.: Stochastic climate theory, arXiv, (last access: 31 Aug 2020), 2016.

Grewal, J. K., Krzywinski, M., and Altman, N.: Markov models – Markov chains, Nat. Methods, 16, 663–664, https://doi.org/10.1038/s41592-019-0476-x, 2019.

Hari, V., Rakovec, O., Markonis, Y., Hanel, M., and Kumar, R.: Increased future occurrences of the exceptional 2018–2019 Central European
725 drought under global warming, Sci. Rep-UK, 10, 1–10, 2020.

Henley, J., Chrisafis, A., and Jones, S.: France records all-time highest temperature of 45.9C, The Guardian, 28 Jun 2019 (last access: 31 Aug 2020), 2019.

Hirt, M., Schielicke, L., Müller, A., and Névir, P.: Statistics and dynamics of blockings with a point vortex model, Tellus A: Dynamic Meteorology and Oceanography, 70, 1–20, 2018.

730 Hong, C.-C., Hsu, H.-H., Lin, N.-H., and Chiu, H.: Roles of European blocking and tropical-extratropical interaction in the 2010 Pakistan flooding, Geophys. Res. Lett., 38, 2011.

Kanamitsu, M., Ebisuzaki, W., Woollen, J., Yang, S.-K., Hnilo, J., Fiorino, M., and Potter, G.: Ncep–doe amip-ii reanalysis (r-2), B. Am. Meteorol. Soc., 83, 1631–1644, 2002.

Kimoto, M. and Ghil, M.: Multiple flow regimes in the Northern Hemisphere winter. Part II: Sectorial regimes and preferred transitions, J.
735 Atmos. Sci., 50, 2645–2673, 1993.

Kuhlbrodt, T. and Névir, P.: Low-order point vortex models of atmospheric blocking, Meteorology and Atmospheric Physics, 73, 127–138, 2000.

Lucarini, V., Freitas, A. C. M., Nicol, M., Freitas, J. M., Todd, M., Faranda, D., Kuna, T., Hollande, M., and Vaienti, S.: Extremes and recurrence in dynamical systems, Wiley, 2016.

740 Markov, A. A.: An Example of Statistical Investigation of the Text Eugene Onegin Concerning the Connection of Samples in Chains, Science in Context, 19, 591–600, https://doi.org/10.1017/S0269889706001074, 2006.

Matlab: MATLAB version 9.0.0.341360 (R2016a), The MathWorks Inc., Natick, Massachusetts, 2016.

McCullagh, P. and Nelder, J. A.: Generalized Linear Models 2nd edition, London, UK, 1989.

Mohr, S., Wilhelm, J., Wandel, J., Kunz, M., Portmann, R., Punge, H. J., Schmidberger, M., Quinting, J. F., and Grams, C. M.: The role of
745 large-scale dynamics in an exceptional sequence of severe thunderstorms in Europe May–June 2018, Weather and Climate Dynamics, 1, 325–348, https://doi.org/10.5194/wcd-1-325-2020, 2020.

Müller, A. and Névir, P.: A geometric application of Nambu mechanics: the motion of three point vortices in the plane, J. Phys. A-Math. Theor., 47, 105 201, 2014.

Müller, A., Névir, P., Schielicke, L., Hirt, M., Pueltz, J., and Sonntag, I.: Applications of point vortex equilibria: blocking events and the
750 stability of the polar vortex, Tellus A, 67, https://doi.org/10.3402/tellusa.v67.29184, 2015.

Newton, P. K.: The N-Vortex Problem: Analytical Techniques, Springer-Verlag, 2001.

Obukhov, A., Kurganskii, M., and Tatarskaia, M.: Dynamic conditions for the origin of drought and other large-scale weather anomalies, Meteorologiia i Gidrologiia, pp. 5–13, 1984.

Pelly, J. L. and Hoskins, B. J.: A new perspective on blocking, J. Atmos. Sci., 60, 743–755, 2003.

755   Pfahl, S. and Wernli, H.: Quantifying the relevance of atmospheric blocking for co-located temperature extremes in the Northern Hemisphere on (sub-) daily time scales, Geophys. Res. Lett., 39, 2012.

Pinheiro, M., Ullrich, P., and Grotjahn, R.: Atmospheric blocking and intercomparison of objective detection methods: flow field characteristics, Clim. Dynam., 53, 4189–4216, 2019.

R Core Team: R: A language and environment for statistical computing, R Foundation for Statistical Computing, Vienna, Austria, https:
760   //www.R-project.org/, 2018.

Rex, D. F.: Blocking action in the middle troposphere and its effect upon regional climate: Part I. An aerological study of blocking action, Tellus, 2, 196–211, 1950.

Richling, A., Kadow, C., Illing, S., and Kunst, O.: Freie Universität Berlin evaluation system (Freva) - Blocking, https://freva.met.fu-berlin. de/about/blocking/, (Documentation of the blocking plugin), Accessed: 2020-09-10, 2015.

765   Russo, S., Sillmann, J., and Fischer, E. M.: Top ten European heatwaves since 1950 and their occurrence in the coming decades, Environ. Res. Lett., 10, 2015.

Scherrer, S. C., Croci-Maspoli, M., Schwierz, C., and Appenzeller, C.: Two-dimensional indices of atmospheric blocking and their statistical relationship with winter climate patterns in the Euro-Atlantic region, Int. J. Climatol., 26, 233–249, 2006.

Schielicke, L.: Scale-dependent identification and statistical analysis of atmospheric vortex structures in theory, model and observation, Ph.D.
770   thesis, Freie Universität Berlin, Berlin, Germany, 2017.

Schielicke, L., Névir, P., and Ulbrich, U.: Kinematic vorticity number – a tool for estimating vortex sizes and circulations, Tellus A, 68, https://doi.org/10.3402/tellusa.v68.29464, 2016.

Schwierz, C., Croci-Maspoli, M., and Davies, H.: Perspicacious indicators of atmospheric blocking, Geophys. Res. Lett., 31, 2004.

Spekat, A., Heller-Schulze, B., and Lutz, M.: Über Großwetterlagen und Markov-Ketten, Meteorol. Rundsch., 36, 243–248, in German,
775   1983.

Sterl, A.: On the (in) homogeneity of reanalysis products, J. Climate, 17, 3866–3873, 2004.

Tibaldi, S. and Molteni, F.: On the operational predictability of blocking, Tellus A, 42, 343–365, https://doi.org/10.1034/j.1600-0870.1990.t01-2-00003.x, 1990.

Truesdell, C.: Two measures of vorticity, Indiana Univ. Math. J., 2, 173–217, 1953.

780   Truesdell, C.: The kinematics of vorticity, Indiana University Press, Bloomington, Indiana, 1954.

Tung, K. K. and Lindzen, R.: A theory of stationary long waves. Part I: A simple theory of blocking, Mon. Weather Rev., 107, 714–734, 1979.

Tyrlis, E. and Hoskins, B. J.: Aspects of a northern hemisphere atmospheric blocking Climatology, J. Atmos. Sci., 65, 1638–1652, https://doi.org/10.1175/2007JAS2337.1, 2008.

785   Vautard, R., Mo, K. C., and Ghil, M.: Statistical significance test for transition matrices of atmospheric Markov chains, J. Atmos. Sci., 47, 1926–1931, 1990.

Wallace, J. M., Zhang, Y., and Lau, K.-H.: Structure and seasonality of interannual and interdecadal variability of the geopotential height and temperature fields in the Northern Hemisphere troposphere, J. Climate, 6, 2063–2082, 1993.

Wilks, D. S.: Statistical methods in the atmospheric sciences, vol. 100 of *International geophysics series*, Academic Press, 3 edn., 2011.

790 Woollings, T., Barriopedro, D., Methven, J., Son, S.-W., Martius, O., Harvey, B., Sillmann, J., Lupo, A. R., and Seneviratne, S.: Blocking and its response to climate change, Current climate change reports, 4, 287–300, 2018.

Yee, T. W.: Vector generalized linear and additive models: With an implementation in R, Springer, New York, USA, 2015.